2011

Development And Characterization Of Thermal Diffusion Doped Fe2+:Znse/Zns Polycrystalline Gain Media For Room Temperature Mid-Ir Lasing

Nosoung Myoung
University of Alabama at Birmingham

DEVELOPMENT AND CHARACTERIZATION OF THERMAL DIFFUSION DOPED FE2+:ZNSE/ZNS POLYCRYSTALLINE GAIN MEDIA FOR ROOM TEMPERATURE MID-IR LASING

by

NOSOUNG MYOUNG

SERGEY B. MIROV, COMMITTEE CHAIR
VLADIMIR V. FEDOROV
MARY ELLEN ZVANUT
SERGEY VYAZOVKIN
PATRICK KUNG

A DISSERTATION

Submitted to the graduate faculty of The University of Alabama at Birmingham,
in partial fulfillment of the requirements for the degree of
Doctor of Philosophy

BIRMINGHAM, ALABAMA

2011

DEVELOPMENT AND CHARACTERIZATION OF THERMAL DIFFUSION DOPED FE2+:ZNSE/ZNS POLYCRYSTALLINE GAIN MEDIA FOR ROOM TEMPERATURE MID-IR LASING

NOSOUNG MYOUNG

DEPARTMENT OF PHYSICS

ABSTRACT

The dissertation is focused on thermo-diffusion doping of Fe^{2+}:ZnSe, Fe^{2+}:ZnS, Fe^{2+}:Co^{2+}:ZnSe, and Fe^{2+}:Co^{2+}:ZnS polycrystals and their laser-spectroscopic characterization. Most materials absorb infrared (IR) light at specific patterns of frequencies directly related to their structure. IR spectra can therefore be used to identify and quantify the constituents of an unknown material, making detection of chemicals by their absorption of IR light an important analytical tool. For instance, Mid-infrared lasers (λ = 3 to 5μm) are widely used for an environmental monitoring, remote sensing of atmosphere and defense-related applications. Tunable middle infrared lasers are essential for highly sensitive detection of organic molecules because the strongest vibrational absorption lines of many molecules lie within middle infrared spectral range. Emerging Fe^{2+}:ZnSe lasers have potential to operate at room temperature over 3-6μm spectral range. The major problem of Fe:ZnSe (ZnS) gain materials is in a lack of cost effective technology of high quality Fe:ZnSe (ZnS) crystals fabrication. We are making a new approach for the fabrication of gain and passive Fe^{2+}:II-VI semiconductor materials with a pre-assigned concentration of Fe^{2+} ions by thermal diffusion from the metal films deposited by a precisely controlled thermal evaporation. This method potentially enables a uniform distribution of iron ions over the crystal volume and offers a good flexibility in optimization of iron concentration. Developed Fe:ZnSe crystals were characterized

spectroscopically as a function of temperature, Fe concentration and thermal diffusion parameters. 3μm pumped gain-switched lasers based on optimal Fe:ZnSe crystals were developed and characterized. We also studied the effect of co-doping Fe:ZnSe (or Fe:ZnS) crystals with Co. Kinetics of luminescence of Fe ions were measured as a function of Co concentration to evaluate the efficiency of energy transfer from Co to Fe ions.

Keywords: thermal diffusion, Transitional Metals, Energy transfer, Mid-Infrared laser, tunable laser

Dedication

This dissertation is dedicated to my family and my wife, JinOk Heo

Acknowledgments

I have always looked forward to writing this part. As it turned out, this moment finally came to me. I hope this part will make you smile.

Many graduate students in Department of Physics, UAB benefit from having a good dissertation advisor to pursuit their careers as a physicist. I have one too who was great. Dr. Sergey B. Mirov has so much anxious to do science especially for optics and lasers. He is the most wonderful professor I have ever known and makes group members challenge right direction on the projects.

I would like to thank Dr. Vladimir V. Fedorov, Dr. Mary Ellen Zvanut, Dr. Sergey Vyazovkin, and Dr. Patrick Kung for carefully reviewing my dissertation. Dr. Fedorov deserves special recognition for the incredible work that he has guided on how to analyze a mountain of data. I will miss his speaking. Whenever he sees me on the right behind me (kind of scaring me all the time), he would ask, “How is going?”

It has been a pleasure to work with Dr. Dmitri V. Martyshkin. I must have knocked his door more than he used to get in the past years to call upon his laser expertise. The thing I would not want to hear from him was “the mirror is broken”. This one sentence delayed my work for months. And I am also thankful to all COSS members, Dr. Igor Moskalev, Anitha Arumugam, Alan Martinez, Tetyana Konak and Jeremy Peppers helping me for experimental set-ups and sample preparations.

I have spent most of time in the lab or in my office during the graduate school year. During that time, I would have not survived without my friendship with all colleagues such as Walter Uhoya Omondi (Kenya), Jonathan Williams (Belize), Chrissy Richey (physics mama), Hyunbin Kim, the late Wonwoo Lee, and so on. They are just as important as the people who supported me in the lab. During the school year, I have learned not only their different cultures, but also their strong friendship. But I still worry about inappropriate influence to Walter from Jonathan like “Oo Hoo~”. Chrissy as a physics mama organized all activities among graduate students. Without her, all graduate students may have not known each other.

Finally, I would like to thank my family. My parents still think that I have gone too far, but I could have not done this work without their strong support from warm hearts. Especially my mother always reminds that my family is right behind me no matter what happens. My younger brother, Nhosik Myoung, is a man of sincerity who takes care of family instead of me. And I deeply appreciate my wife, JinOk Heo, who believes and supports me.

CH315, Birmingham, AL, March 2011

TABLE OF CONTENTS

Page

LIST OF TABLES

Table *Page*

LIST OF FIGURES

Figure *Page*

CHAPTER 1

INTRODUCTION TO Mid-IR LASERS

1.1 Introduction

For more than two decades, a significant effort has been made in the development of novel mid-IR lasers promising for a wide range of applications such as free space optical communication, remote sensing [1], material diagnostics [2] etc. Although various mid-IR lasers have been developed, the majority of them have not been commercialized due to a limited output power and difficulty to operate and maintain performance at room temperature. There have been several approaches to develop laser sources for mid-IR spectral region such as molecular gas lasers, optical parametric oscillators (OPO), semiconductor quantum cascade lasers [3,4], etc.

One of the most promising approaches to reach mid-IR spectral range is based on direct lasing of transition metal (TM) doped II-VI wide band semiconductors [5,6]. In 1996, the researchers in the Lawrence Livermore National Laboratory first introduced TM^{2+} chalcogenides as gain materials promising for room temperature broadly tunable mid-IR lasing. [7]. Since then many research groups focused their efforts towards study of these materials and designing lasers on their basis. The major effort was related to Cr^{2+} doped chalcogenide lasers as attractive sources of tunable laser radiation in the 2-3 μm spectral region [8,9,10,11]. Cr^{2+}:ZnSe and Cr^{2+}:ZnS lasers have been of high interest due to their broad tunability over 1.9-3.3 μm spectral range at room temperature, high optical

efficiencies and potential to be scaled to high (>10W) powers via direct fiber or diode pumping [12,13]. Recently a progress has been also demonstrated for Fe^{2+} doped II-VI crystals [14,15,16,17,18,19,20] promising for room temperature tunable mid-IR lasing over 3 to 6 μm spectral range. Low temperature lasing of Fe:ZnSe crystals was achieved over 15-180 K temperature range [21]. A continuous-wave oscillation of Fe:ZnSe laser at liquid-nitrogen temperature was reported in [22]. The first room temperature Fe:ZnSe lasing in gain-switched operation mode with tuning over the 3.9-4.8 μm spectral range was demonstrated in [23]. However, the maximum documented single-pulse energy in the gain-switched regime of operation with *ns* pulse durations has been only several hundreds of μJ for many years [24,25]. Fe^{2+}:ZnSe laser energy scaling was reported recently in [26]. With the use of Fe:ZnSe gain element grown by Bridgman-technique the output energy reached 1.2 mJ level at 4.5 μm and 65 *ns* pulse duration. Likewise, a detailed interpretation of the optical absorption spectrum of Fe^{2+} in cubic ZnS was first introduced at temperature near 300 K by W.W. Coblentz [27, 28]. Lately, a laser based on a Fe^{2+}:ZnS crystal was demonstrated at room temperature at the spectral tuning range over 3.49-4.65 μm for the first time by V.I. Kozlovsky [29]. The major problem with the output energy scaling-up was in the development of fabrication technology for large-aperture, good optical quality, high optical density Fe:ZnSe (ZnS) gain elements and in a lack of high energy pump sources.

1.2 Motivation

Semiconductor materials of the II-VI group of periodic table feature a wide range of optical and electrical properties, and have been successfully used in a variety of

optoelectronic applications such as light emitting diodes (LEDs) as well as lasers. These un-doped bulk II-VI materials such as ZnSe, ZnS, CdSe and ZnTe have a wide transparency window in the near and mid-infrared spectral regions. When transition metal ions (TM^{2+}) such as Ti^{2+}, V^{2+}, Cr^{2+}, Mn^{2+}, Fe^{2+}, Co^{2+}, Ni^{2+} etc (also known as transition metals) are introduced into II-VI semiconductor materials by various growing or doping methods, they feature chemically stable divalent charge state due to substitution in T_d symmetry lattice sites of II-VI crystals without the need for charge compensation.

In addition, tetrahedral crystal field splitting and strong electron-phonon coupling lead to formation of deep energy levels in the forbidden gap, with ^5E being the ground state and $^5T_2$ as the first excited state for Fe^{2+} (vice versa for Cr^{2+}) featuring broad absorption and emission bands in the mid-IR spectral range. It has been known that the iron-related recombination processes give rise to characteristic $^5E \rightarrow {}^5T_2$ intra center mid IR emission of Fe^{2+} over 3~6 μm spectral range [30] as shown in Figure 1-1. Cobalt co-doped ZnSe and ZnS experience thermal quenching and low quantum yield efficiency. On the other hands, Co^{2+}:ZnSe single crystal was revealed as a potentially promising saturable absorber for giant-pulse eye-safe lasers operating at 1.55μm [31]. The nature of the recombination processes has been discussed in numerous publications [32,33]. Mid-IR laser effects in the range of 3~5 μm have been reported for Cr^{2+}:ZnSe [34,35,36,37], Cr^{2+}:ZnS [34,35], Cr^{2+}:CdTe [38], Cr^{2+}:CdSe [39], Fe^{2+}:ZnSe [40] and Fe^{2+}:ZnS [41]. These laser materials have a wide bandgap and possess several noticeable features. One of them is tendency to crystallize as tetrahedrally coordinated structures which enable smaller crystal field splitting than for ordinary octahedral coordinated structures, pushing the dopant transitions further into infrared regions. Another key feature of these materials

is that the heavy anions in the crystals provide a very low energy optical phonon cut-off that makes them transparent in a wide spectral region and decreases the efficiency of non-radiative decay, which gives a promise of a high yield of fluorescence at room temperature.

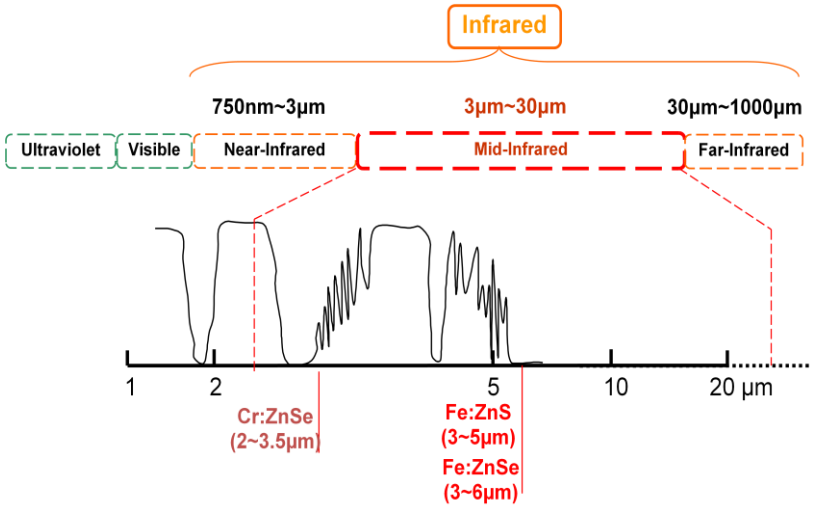

Figure 1-1. Atmospheric transmission and the range of tunability of Fe:ZnSe laser.

1.3 Problem statement and objectives

Tunable solid state lasers are of interest for a wide range of applications such as scientific research, medicine, measurement and testing techniques, and communications. These laser media based on the direct oscillation of crystals doped with rare-earth (RE) and transitional metal ions (TMs) have covered the wavelength between 0.27μm (for Ce^{3+}:LiCAF) [42] and 4.5μm (for Fe^{2+}:ZnSe, pulsed, 180K). There is a high demand for tunable middle infrared lasers having radiation overlapping with 2-10μm molecular "fingerprint" spectral range. For instance, 3 to 3.5nm laser sources are important for various applications including gas sensing, spectral analysis, infrared illumination, countermeasures, medical diagnostics, and others. When tuned to wavelengths between 6μm and 7μm, such lasers are promising for medical applications and removing defined volumes of soft tissue with a very little collateral damage [43]. In order to realize these middle-infrared tunable lasers, a lot of experimental efforts are needed to find crystal hosts with a small phonon cut-off for high efficiency of fluorescence at room temperature as well as to optimize technology of their fabrication. Recent performance of Cr^{2+} doped zinc chalcogenides under continuous wave or pulsed optical excitation has been well documented in the literature [44,45]. The first lasing action of Fe^{2+} doped InP at 2K was demonstrated by Klein *et al* [46], while the first tunable (3.98 and 4.5μm) lasing of Fe:ZnSe crystals over 15 to 180K temperature range was demonstrated in [21]. Recently Fe:ZnSe laser continuously tunable between 3.98 and 4.5μm spectral range was performed at 255K [47]. There have been many suggested fabrication methods for TM doped II-VI. For instance, Cr and Fe doped II-VI crystals can be directly grown from melt using vertical Bridgman technique [48,49]. However, due to sublimation of II-VI

material at temperatures much smaller than melting temperature, this technology requires simultaneous application of high temperature and pressure and, hence, is not commercially viable.

Notable technologies used to fabricate mid-IR gain elements are mainly based on post-growth thermal diffusion of active impurities (e.g. Cr and Fe) in II-VI crystals grown by physical or chemical vapor transport (PVT, CVT) methods [50]. In addition, high vacuum pulsed laser deposition (PLD), molecular beam expitaxy (MBE), and chemical vapor deposition (CVD) are used to grow thin film structures [51,52,53]. The first method (PVT) enables high optical quality of grown crystals. However, the problem of PVT is in a difficulty to realize a sufficiently high concentration of TM dopants [54]. The Bridgman method also has difficulty in obtaining homogeneously doped crystals [55]. One disadvantage of MBE and PLD is that they are not appropriate for fabrication of bulk samples. Therefore it is desirable to review alternative technological methods for cost-effective fabrication of high quality TM doped gain materials. Our research group has been focused on post-growth thermal diffusion of transition metal ions (e.g. Fe and Co) in II-VI compounds from the metal phase deposited by thermal evaporation technique. The properties of thin films are critically dependent on the deposition method and the experimental conditions involved. Optimization of deposition parameters and study of thermal diffusion of Fe ions in II-VI materials is one of the major objectives of current research. Another major problem to be addressed is whether TM dopants, such as Fe^{2+}, are promising for effective broadly tunable lasing at room temperature. Finally, Fe:II-VI lasers feature another problem - a lack of convenient pump laser. With this regards, capitalizing on the fact that characteristic Co^{2+}emission nicely overlaps with Fe^{2+}

absorption and possibly enables energy transfer from Co to Fe ions, we want to study Co-Fe energy transfer parameters in ZnSe and ZnS crystals to potentially realize a laser with a convenient 0.74 or 1.6μm pump sources.

The objectives of my research were as follows:

1. Study of Fe thermal diffusion process from the iron metal film in ZnSe and ZnS crystals as well as determination of the diffusion constant.
2. Optimization of diffusion parameters for development of large-size homogeneously doped Fe:ZnSe and Fe:ZnS laser elements.
3. Optical characterization of the highly doped Fe:ZnSe samples.
4. Optical characterization of the Fe:ZnS samples.
5. Scaling-up of the output energy of the room temperature Fe:ZnSe lasers based on developed samples.
6. Study of the energy transfer process in the co-doped Co:Fe:ZnSe samples.
7. Realization of the new excitation mechanism of Fe^{2+} lasers via energy transfer from Co^{2+}.

CHAPTER 2

TRANSITION METAL DOPED II-VI CHALCOGENIDE LASER CRYSTALS STATE-OF-THE-ART

2.1 Properties of II-VI semiconductors

Transition metal doped II-VI compound semiconductors have been known as promising mid-IR gain materials. These host crystals (such as ZnSe, ZnS, and ZnTe *etc*) show a wide range of optical and electrical properties which make them also promising candidates for optoelectronics and molecular spectroscopy applications [56,57].

One of the interesting infrared II-VI host materials is ZnSe (Zinc Selenide) featuring a wide energy band gap of 2.7eV at 300K [58], low passive loss, and broad transparency in the near and mid-infrared spectral regions. These advanced features define its wide use as a material of choice for IR windows, lenses and prisms. It has superior optical transmission with low bulk losses from scatter and absorption. The second material of interest is ZnS (Zinc sulfide). Like ZnSe, its technology of fabrication is well developed and enables high optical quality and low loss crystals, making it another passive material of choice for IR technology. ZnSe and ZnS are also promising hosts for mid-IR gain materials and the main host crystals in this work. The third II-VI crystal of interest is ZnTe (Zinc Telluride). It has an optical band gap of 2.26eV at room temperature [59] and can be considered as another promising material for mid-IR laser sources. Absorption and emission spectroscopy of $^5E(D) \leftrightarrow {}^5T_2(D)$ infrared transitions of $Fe^{2+}(d^6)$ ions in these host crystals has been reported at liquid-helium temperature [60].

The energy bandgaps for chacogenide crystals and schematic energy diagrams [61] for Cr^{2+} and Fe^{2+} ions in ZnSe are shown in Figure 2-1 (top and bottom, respectively).

To be successfully used as gain media these materials should possess the tendency to crystallize as tetrahedral structures which results in smaller crystal field splitting, leading the dopant transitions to the IR. Also, the heavy anions in the crystals provide a very low energy optical phonon cut-off that makes them transparent in a wide spectral region and decreases the efficiency of non-radiative decay. This gives a promise of a high yield of fluorescence at room temperature.

2.2 Role of impurities in II-VI crystals

Many experimental and theoretical studies lack a comprehensive and quantitative understanding of the electronic structure of the TM centers. In this paragraph, a comprehensive overview of the TM centers in a wide range of II-VI host materials is presented and crucial information required for feasibility of Fe based mid-IR laser sources development is shown.

S. Kuck has summarized the laser relevant data of some crystals doped with ions of different configurations [62]. In Table 1, the transition metal ions in octahedral and tetrahedral coordination are listed according to their corresponding energy level diagram (i.e. Tanabe-Sugano diagram).

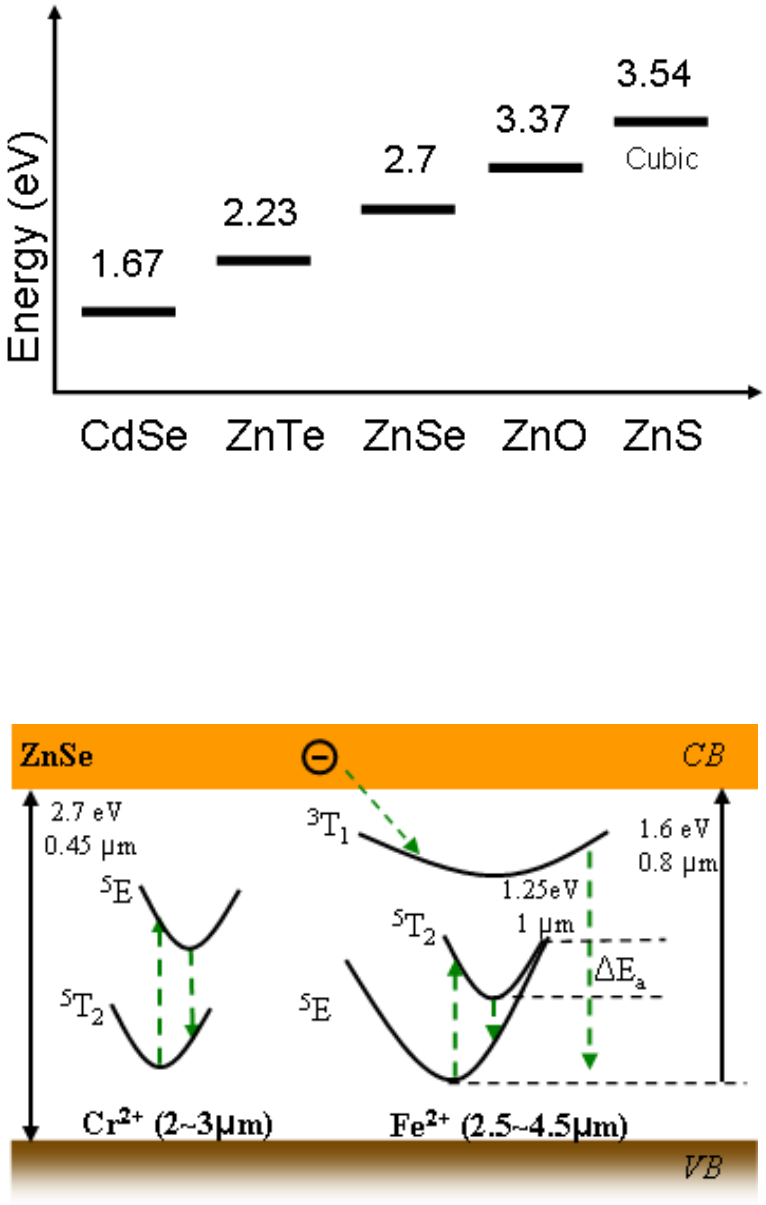

Figure 2-1. Energy band gap *vs.* chalcogenide crystals (top) and configuration coordinate diagrams of Fe and Cr ions in ZnSe (bottom).

The laser active ions are indicated using (a) or (b) superscripts. Concerning laser oscillation the d^3 and the d^8 diagrams are the most favorable. In the case of d^1, d^2, d^6, and d^7 configurations only a few ions featured laser action. For ions corresponding to the d^4, d^5 and d^9 configurations, laser oscillation has not been observed.

Table1. Transition metal ions sorted according to the corresponding Tanabe-Sugano diagram (TSD-d^m). Normal: octahedral coordination; Italic: tetrahedral coordination, (a) laser oscillation in octahedral coordination, (b) laser oscillation in tetrahedral coordination

Ion	TSD-d^1	TSD-d^2	TSD-d^3	TSD-d^4	TSD-d^5	TSD-d^6	TSD-d^7	TSD-d^8	TSD-d^9
Ti	$Ti^{3+(a)}$	Ti^{2+}							
V	V^{4+}	V^{3+}	$V^{2+(a)}$					V^{3+}	V^{4+}
Cr		Cr^{4+}	$Cr^{3+(a)}$	Cr^{2+}		$Cr^{2+(b)}$		$Cr^{4+(b)}$	Cr^{5+}
Mn		Mn^{5+}	Mn^{4+}	Mn^{3+}	Mn^{2+}, Mn^{2+}	Mn^{3+}		$Mn^{5+(b)}$	Mn^{6+}
Fe				Fe^{2+}	Fe^{3+}, Fe^{3+}	Fe^{2+}		Fe^{6+}	
Co			Co^{2+}	Co^{3+}		Co^{3+}	$Co^{2+(a)}$		
Ni		Ni^{2+}	Ni^{3+}				Ni^{3+}	$Ni^{2+(a)}$	
Cu	Cu^{2+}							Cu^{3+}	Cu^{2+}

A multiplet structure of transition metal ions (e.g. V^{2+}, Cr^{2+}, Mn^{2+}, Fe^{2+}, Co^{2+}, Ni^{2+}) in II-VI crystals has been studied by A. Fazzio et al. [63, 64, 65, 66, 67]. It was revealed that among all the considered ions Cr^{2+} and Fe^{2+} are the most promising for effective broadly tunable middle-infrared lasing. The major considerations for this conclusion were as follows.

a) The first excited levels of all considered ions except Mn^{2+} lie at an appropriate energy to generate mid-IR emission.

b) The ground and first excited levels of all the considered ions except Mn^{2+} have the same spin, and therefore will have a relatively high cross-section of emission.

c) Higher lying levels of only two ions - Cr^{2+} and Fe^{2+} - have spins that are lower than the ground and first excited levels, greatly reducing the potential for significant excited state absorption at the pump or laser transition wavelengths.

d) The orbital characteristics of the ground and first excited levels for Cr^{2+}, Fe^{2+} and Co^{2+} are different. It is expected that they will experience a significant Franck-Condon shift between absorption and emission, resulting in broadband "dye-like" absorption and emission characteristics, suitable for a broadly tunable laser.

Among these TM:II-VI materials, Fe doped laser crystals are our main focus of investigation. According to the Hund's rule, the ground state of Fe^{2+} free ion is the 5*D* multiplet with the orbital momentum L=2 and the spin S=2, yielding the degeneracy of the ground level $(2L+1)(2S+1)=25$. This manifold is split in a tetrahedral crystal-field potential into the orbital ^5E doublet and the $^5T_2$ triplet. Further detailed influence of the spin-orbit interactions is described in Ref. [68]. The reported zero phonon line (ZPL) for tetrahedral crystal-field for Fe^{2+} in ZnSe material was 2747cm^{-1}, followed by a second ZPL separated by 23cm^{-1} at 4K from the first one [69].

In the following section, we will introduce how the Fe^{2+}:ZnSe crystals could be fabricated and utilized as Mid-infrared amplifying media.

2.3 Methods of fabrication of mid-IR gain media based on TM doped ZnSe & ZnS polycrystals

Many solid state laser gain media are doped with TM ions and those ions have been of great interest because of their broadband emission. Those media have optical transitions that involved the electrons of the 3*d* shell (Fe: (*Ar*) $4s^2 3d^6$, Cr: (*Ar*) $4s^1 3d^5$). Previously, ZnS and ZnSe were used as host materials for chromium to produce mid-IR lasing over 2-3μm spectral range. Compared to these materials, Fe^{2+}:ZnSe media, capable to cover 3-6μm (3-5μm for Fe:ZnS) spectral range, represent emerging technology that requires a lot of efforts for high quality Fe:ZnSe (ZnS) crystals fabrication. Currently, the state of the art in TM:II-VI laser systems relies either on single crystal, or vapor grown polycrystalline materials [70,72,75]. Both of these materials have particular drawbacks in terms of crystal doping. The commonly used doping methods are based on growth from melt, vapor growth, or after growth thermo-diffusion doping. Under atmospheric pressure ZnSe sublimation occurs at a temperature above approximately 400 ℃ which is much lower than the melting point temperature (1538 ℃). Therefore, in order to make use of melt growth techniques, in addition to a high temperature (1538 ℃), it is necessary to apply high pressure ($75x10^2$ KPa). High temperature melt growth is often accompanied by uncontrolled contamination. This contamination can lead to unexpected and parasitic absorptions. Control of the amount of Fe^{2+} ions incorporated in the crystal is also difficult with the use of vapor growth techniques. Doping of host crystals (polycrystals) that are already grown allows for another method of TM incorporation, which is known as thermal diffusion. This technique utilizes thermally activated diffusion of transition metal

ions into the II-VI crystals. This diffusion can be performed from the gas, liquid, or metal phase.

We hypothesize that the most effective route for obtaining pre-assigned TM impurity concentration in the crystal is diffusion from the metal thin film evaporated on the surface of II-VI crystal. There are three methods of evaporation techniques.

1) The first is e-beam evaporation - an electron beam is aimed at the source material causing local heating and evaporation.
2) The second is plasma sputtering, widely used for making films of alloys and high melting temperature metal materials.
3) The third is a resistive evaporation which consists of a tungsten spiral filament, containing the source material (such as iron or cobalt) electrically heated with a high current to make the material evaporate.

In this work, our mainly used doping method is based on thermal evaporation (TE) techniques using resistively heated tungsten filament in high vacuum system and will be addressed in chapter 3.

CHAPTER 3

STUDY OF THE THERMAL DIFFUSION OF IRON IN ZnSe AND ZnS FROM METAL PHASE

Optimization of thermal diffusion parameters has been performed by measurement of gradient of Fe distribution over the crystal volume as a function of temperature and annealing time. The diffusion process of iron in the host can be described using *Fick's 2nd law*:

$$\frac{\partial C}{\partial t} = \nabla \cdot \left(D \nabla C \right) \tag{3-1}$$

where $C(r,t)$ is concentration of the dopant ions and D is a diffusion coefficient. There are two important boundary-initial conditions for practical applications in the case of one-dimensional geometry. First is diffusion with constant surface concentration *C(0)* when host occupies the half-space (semi-infinite media, $x>0$). This condition is usually realized in the diffusion from the gas phase when host is annealed in the dopant vapor at constant pressure. In this case solution of the diffusion equation can be written as:

$$\mathrm{C(t,x)} = \mathrm{C(0)} \cdot \mathrm{erfc}\left(\frac{\mathrm{x}}{2\sqrt{\mathrm{D}\cdot\mathrm{t}}}\right) \tag{3-2}$$

where the abbreviation is

$$\mathrm{erfc(z)} \approx 1 - \frac{2}{\sqrt{\pi}} \int_0^{\mathrm{z}} \exp\left(-\eta^2\right) \mathrm{d}\eta \tag{3-3}$$

Second commonly encountered initial condition is so-called instantaneous planar source:

$$C(t = 0, x) = M\delta(x) \tag{3-4}$$

It describes experiments with initial condition when thin-film layer of the dopant is deposited on the host surface before annealing. M denotes the number of the dopant ions per unit area. The solution of the diffusion equation in this case can be written as:

$$C(x, t) = \frac{M}{\sqrt{\pi Dt}} exp\left(-\frac{x^2}{4Dt}\right) = \frac{bC_0}{\sqrt{\pi Dt}} exp\left(-\frac{x^2}{4Dt}\right) \tag{3-5}$$

where, C_0 is concentration of atoms in the deposited film, b is a film thickness, and t is annealing time. The characteristic value of $2\sqrt{Dt}$ is usually defined as a diffusion length.

In our work we studied thermo-diffusion of the TM ions in ZnSe and ZnS materials from the metal film deposited on the crystal surfaces.

3.1 Optimization of thermal evaporator for Fe thin film deposition

The technique of thermal evaporation has been used for large and small area deposition of Fe on single and polycrystalline ZnSe substrates placed at sufficient distance from the evaporator to guarantee uniformity in film composition and thickness. Iron metal pieces (pellets) are evaporated from resistively heated tungsten filament sources.

Each deposition rate is monitored by Quartz crystal thin film sensor. The main advantages of this process are high volume deposition rates and relatively low substrate temperatures. The major features of a conventional thermal deposition system are depicted Figure 3-1.

The metal species are evaporated on the surface of II-VI semiconductors in high vacuum. Normally, the chamber is pumped to $5x10^{-7}$ Torr using diffusion pump. The diffusion pump operates to 10^{-7} Torr featuring relatively high pumping speed by boiling a

fluid (hydrocarbon oil), and forcing the dense vapor stream through central jets angled downward to give a conical curtain of vapor. Gas molecules from the chamber that randomly enter the curtain are pushed toward the boiler by momentum transfer from the more massive fluid molecules. During the deposition, ballistic propagation of the vapor requires a residual gas background with pressure below 10^{-5} Torr.

Evaporation source materials for our experiments are mostly Fe available in various forms such as pellets, rods or powders. The distance between the source and substrate can be chosen approximately in the range of 10 to 15 cm and automatically results in a high uniformity of the deposited film. The sources are heated via a resistive filament under vacuum to their melting point and give off a vapor, the atoms of which have some temperature dependent kinetic energy. The source atoms travel in a straight line from the source to the sample.

In order to obtain a homogeneous temperature distribution across the entire substrate area, substrate holder requires an optimal heating system which contains two 300W HALOGEN projector lamps. The substrate temperature is controlled with a thermocouple and is maintained at 300-350 ℃. The optimized substrate temperature will be shown in the next paragraph devoted to thermal diffusion calculations.

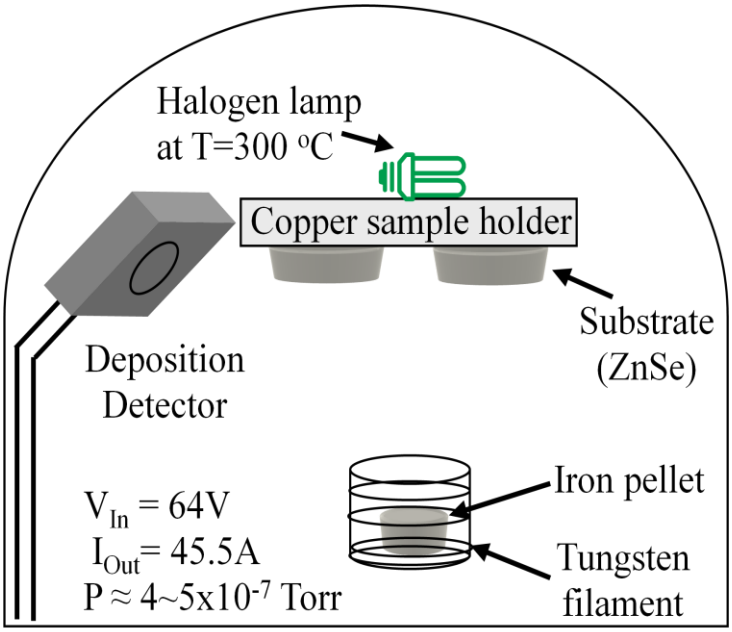

Figure 3-1. General schematics of the thermal evaporator

Thermal evaporation techniques are well designed to create a controlled concentration of TM ions in II-VI compounds. TE used in this work has capability to deposit Fe films of thicknesses ranging from 10 nm to 2 μm. The samples were prepared either with one side or both sides Fe deposition process (sandwich geometry) by TE. Once the substrate has been deposited with Fe thin film in a high vacuum, the samples were sealed in a silica quartz ampoule under high vacuum (P < 10^{-4} Torr), placed in a furnace, heated up within about 2 hours to ~ 1000 ℃, and finally annealed at 1000℃ for a few days. In order to keep the temperature uniformity, the ampoules are placed in the center of the furnace.

There are two ways to deposit impurities on a given substrate; (1) one side deposition and (2) sandwich geometry deposition. One side deposition can be used for the

measurement of diffusion parameters and sandwich geometry deposition can be used for homogeneous impurity distribution in a thick host crystal. A more detailed experimental description will be given in the subsequent sections.

At this point, during the annealing processes of the crystals with one side deposited thin film as shown in Figure 3-2(A), the diffusion takes place from both metal and gas phases. It means that the un-deposited substrate facet is also affected by diffusion from the gas phase. However, the effect from the gas phase from deposited films was minute comparing to the metal phase diffusion. Figure 3-2(B) shows that Fe thin films were deposited on both sides of the sample (sandwich geometry) in order to maintain the homogeneous distribution of doped ions through the host crystals. The characterization of diffusion process and gradient of Fe concentration in ZnSe will be discussed in the following section.

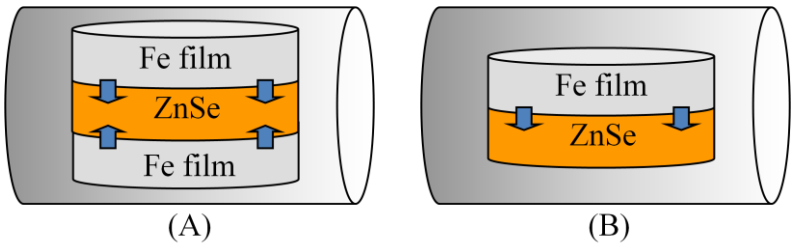

Figure 3-2. Schematics of deposition types; (A) Thin film deposited on both sides of the crystal; (B) One side deposition of thin film.

3.2 Control of Fe thin film deposition

In order to control the film thickness, the evaporation rates are monitored by INFICON XTM/2 deposition monitor through deposition detector (crystal sensor). With a frequency resolution of 0.1 Hz in only 250 ms, the Quartz crystal monitor, when set to 16 second averaging, accurately displays rate resolutions as small as 0.01 Å. It is quite

robust and easy to handle and even for rates of a few Å/sec, the accuracy is in the range of a few percent. Quartz crystal sensor has been calibrated using Park Systems atomic force microscope (AFM) recently purchased by the COSS center (the Center for Optical Sensors and Spectroscopies). Calibration of the crystal monitor is as follows. The density of the added material allows conversion of the mass information into thickness. First, the substrate is placed near the sensor, so that the same thickness will be accumulated on the crystal and the substrate. The density to the bulk value of the film material is set, Z-ratio which is the parameter correcting the frequency change to thickness transfer function for the effects of acoustic impedance mismatch between the crystal and the coated material is set to 1.00 and tooling to 100%. After making a short deposition, the film thickness is measured by AFM. Then, the new density value is determined by

$$Density\ \left(\frac{g \cdot m}{cm^3}\right) = D_1\left(\frac{T_x}{T_m}\right), \tag{3-6}$$

where D_1 is initial density setting as 7.860 gm/cm^3, T_x is thickness reading on the display, and T_m is measured thickness. Once the new density value is estimated, new tooling factor should be calculated from the relationship as

$$Tooling\ (\%) = TF_i\left(\frac{T_m}{T_x}\right), \tag{3-7}$$

where TF_i is the initial tooling factor.

Thin film deposition rate and substrate temperature have been optimized by choosing parameters providing the most uniform thin film thickness, compared by AFM data, and the best film adhesion, controlled by stability of the film during crystal rapid heating in vacuum condition. The thickness from deposition monitor has been compared with the one from Atomic Force Microscope (AFM, Park Systems) for the precise concentration calculation of Fe on ZnSe.

For the optimization of the deposition monitor, two Fe thin film deposited ZnSe substrates were prepared with the thickness from the deposition monitor 1050 nm and 1350 nm. Then, the thickness of thin films was measured by AFM to ensure the exact concentration of Fe deposited on the substrate. As shown in Figure 3-3, sample (left) was estimated for 1020 nm and sample (right) for 1305 nm by AFM which give rise to ± 2~3% error between deposition monitor and AFM thickness measurement.

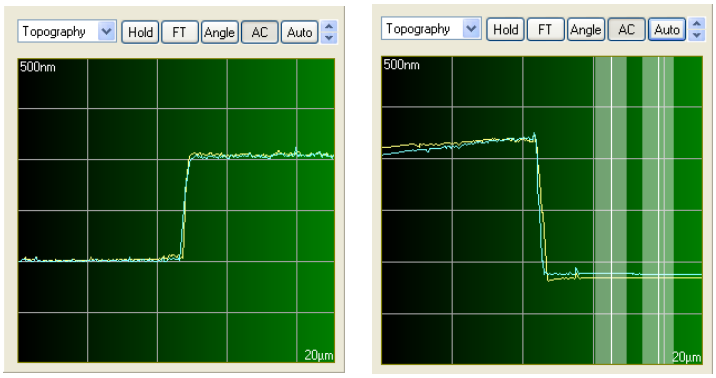

Figure 3-3. Topography by AFM; sample (left) indicates 1020nm while sample (right) shows 1305 nm (each grid has 500nm division)

The detail schematics of AFM are shown in Figure 3-4. AFM has the ability to rule out topographical artifacts mixed in with other physical properties as well as to characterize the surface topography (scan size: 5 μm-left and 10 μm-right) of thin films deposited by thermal evaporation technique on substrates heated to 300-350 °C. The iron thin films on II-VI crystals deposited by TE method have reasonably good quality and mirror like surface morphology. The head mode was chosen to be a contact mode (or a non-contact mode) which enables the ultimate resolution and measurement accuracy, and scan rate was normally applied as 0.5 Hz. The measured grain size was approximately 250-300 nm.

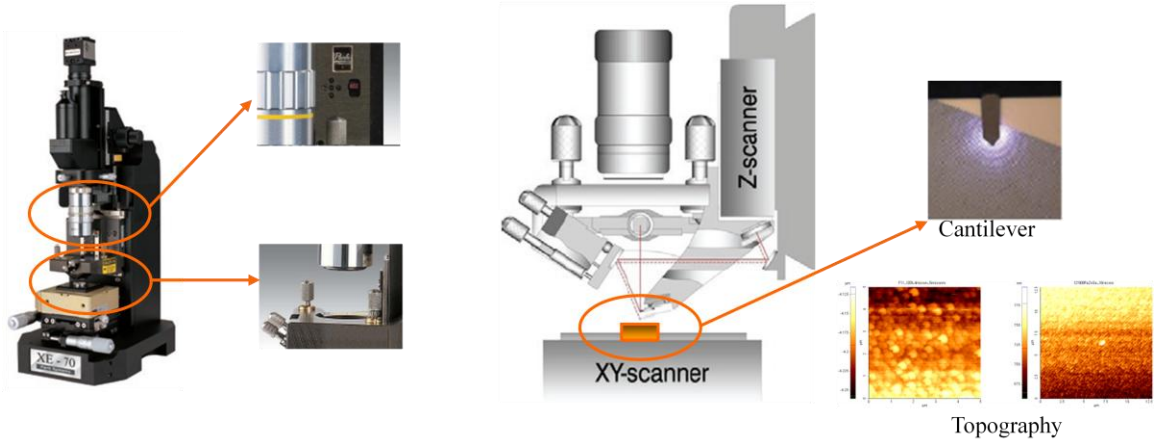

Figure 3-4. AFM schematics and topography of Fe films on ZnSe.

As the atomic mass and density of Fe is known as 55.847 g/mol and 7.874 g/cm^3, respectively, the relation between Fe thin film thickness and Fe concentration for different thicknesses of a host crystal can be easily depicted as shown in Figure 3-5. For this calculation, the thickness of host crystals such as ZnSe or ZnS varied over 0.2-1.0 cm range.

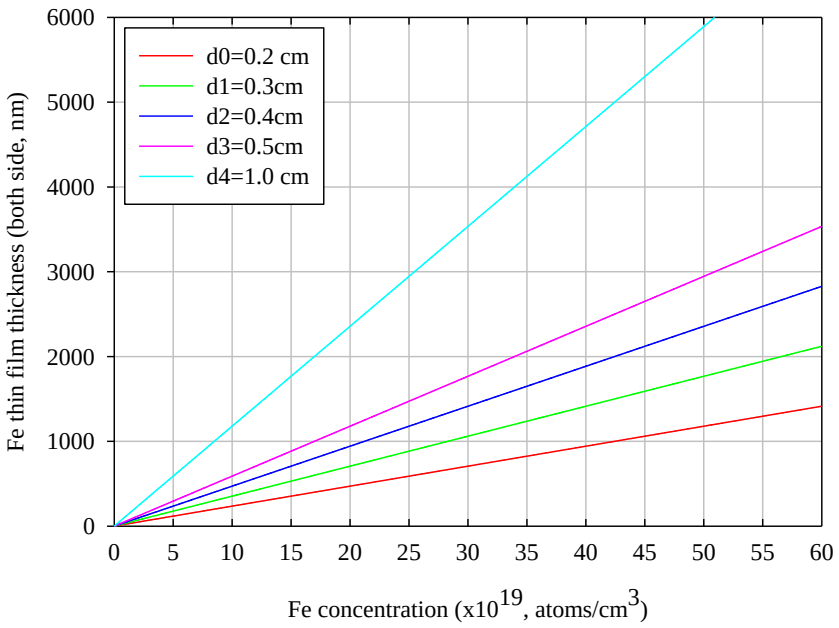

Figure 3-5. Estimation of Fe concentration *vs*. thin film thickness.

3.2.1 Measurement of gradient of Fe^{2+} concentration

After thermal annealing, the iron concentration gradient was studied via spatially resolved measurement of Fe^{2+} IR absorption band. The absorption coefficient measurement at room temperature was carried out along the c-axis by using a spectrophotometer in the range of visible and mid-infrared spectral regions with "Shimadzu UV-VIS-NIR-3101PC" and Bruker "Tensor-27" FTIR spectrophotometers before the sample was cut into 3 pieces to measure the gradient of Fe^{2+} in ZnSe. The thin film deposited facets of Fe^{2+}:ZnSe were inspection polished for the transmittance measurement.

The absorption coefficient α(x,y,z,t) of the samples can be expressed in terms of the doped TM ion concentration N(x,y,z,t) and absorption cross-section σ according to

$$\alpha(x, y, z, t) = \sigma(\lambda)\, N(x, y, z, t)\,, \tag{3-8}$$

where *x, y, z* are the positions inside the host and *t* is diffusion time. In the experiments, we measured the absorbance of the samples. At any given wavelength the measured absorbance ($log(I/I_0)$) has been shown to be proportional to the molar concentration of the absorbing species and the thickness of the sample. After the determination of the background losses ($\alpha_{\text{Fresnel Loss}}$), due to surface imperfections and Fresnel reflections, the average absorption coefficient $\alpha_{\text{ave.}}$ was determined by using

$$\alpha_{ave.} = \frac{1}{d}\ln\left(\frac{1}{T}\right) - \alpha_{FresnelLoss}, \tag{3-9}$$

where d is the thickness of the crystal and T is the transmission. Based on these calculations, Fe:ZnSe crystals gradient of absorption was studied with the use of free running 2.78μm radiation of Er:Cr:YSGG laser (Yttrium-Scandium-Gallium Garnet

crystals co-doped with chromium and erbium). The laser head, depicted in Figure 3-6, consisted of 73 mm long Er:Cr:YSGG crystal with a 3 mm diameter placed at one focus of a gold elliptical chamber and xenon flash-lamp at the other focus.

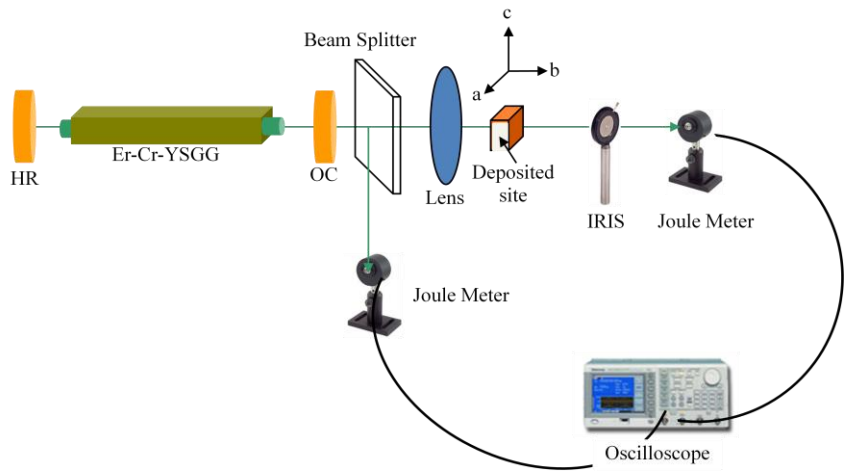

Figure 3-6. Er:Cr:YSGG laser setup for gradient measurement.

The experimental setup consists of a 100% high reflection mirror (HR) and 82% reflective output coupler (OC). The HR was placed 69 mm from the end of the Er:Cr:YSGG laser crystal, and the OC was placed 53 mm from the laser crystal. Input flashlamp pump energy has been determined by directly measuring the voltage across the flashlamp and then calculating the energy delivered to the flashlamp using

$$E = \frac{1}{2}CV^2 \tag{3-10}$$

The output energy is measured by two separated Joule meters and converted to energy dividing the power by the repetition rate of the laser: one for initial transmitted intensity (T_0) and the other for transmitted intensity (T) through the sample.

The beam waist measurement of the 2.78μm radiation of the Er:Cr:YSGG laser has also been performed. The laser beam is focused on the sample by using a convex lens with a focal length 10cm. The pump spot size distribution ω(z) around the focus is measured with the knife-edge technique [71]. The least-squares fitting was employed to the experimental data to estimate the pump spot size distribution by using the following equation

$$\omega(z) = \omega_0 \sqrt{1 + \left(\frac{Z - Z_f}{Z_R} \right)^2}, \tag{3-11}$$

where ω_0 is the beam waist, Z_R is the Rayleigh range, and Z_f is the beam waist location. The beam waist was determined as being approximately 130 μm. The data from two separated Joule meters are collected by a digital oscilloscope (Tektronix TDS 5104) and analyzed by Mathematica 6.0 as shown in Figure 3-7.

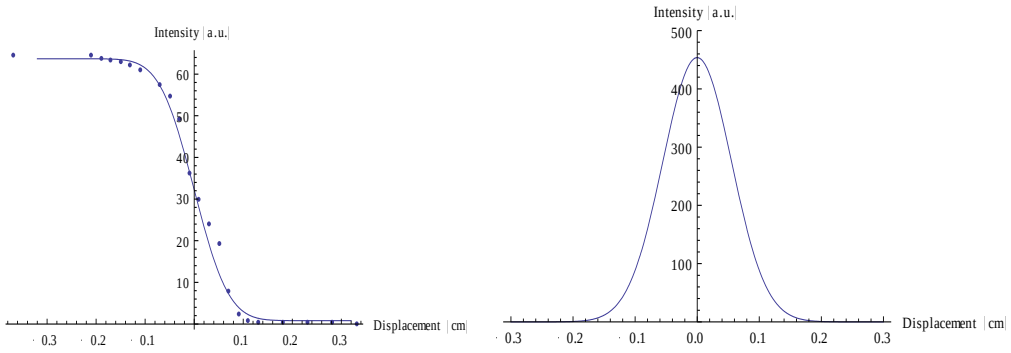

Figure 3-7. Beam waist analysis by Mathematica.

In order to measure the gradient of Fe^{2+} in ZnSe, the data were taken along c-axis representing direction of Fe diffusion through the crystal as shown in Figure 3-8.

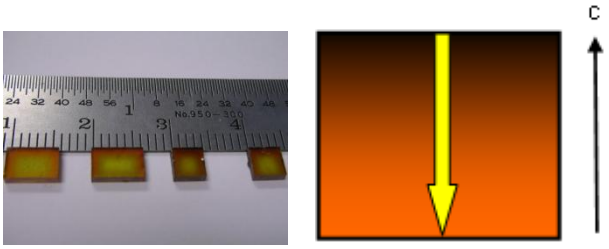

Figure 3-8. Gradient measurement diagram.

The data were converted into the transmittance (*T*). Then the data were transformed from transmission to absorption coefficient (α, [cm^{-1}]). Subsequently the Fresnel absorption was subtracted to obtain the absolute value of α and number of impurity atoms occupied per volume as depicted in Figure 3-9. In this figure, the Fe:ZnSe sample was 6.5mm long which corresponds to the scan displacement on the x-axes. Free running Er:Cr:YSGG was utilized to scan the samples and Fe ions distribution in ZnSe was well defined.

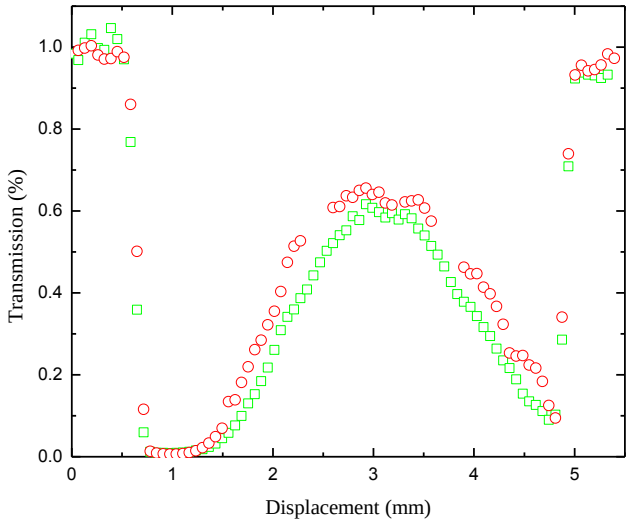

Figure 3-9. Gradient measurement for Fe in ZnSe by Er:Cr:YSGG.

3.3 Optimization of thermal diffusion parameters

3.3.1 Thermal diffusion conditions

Prior to the thermal diffusion of iron thin films in a host crystal, it was realized that surface pre-cleaning and temperature of substrates play a critical role in diffusion process. For the optimization of the substrate cleaning, three different cleaning methods were applied to four ZnSe polycrystals with 10 x 10 mm transverse dimensions and 6 mm thickness. All samples were immersed in each chemical for 5 minutes. Sample (a) was treated in acetone and methanol, while sample (b) was exposed to ultrasonic treatment in distilled water following by methanol cleaning. Samples (c) and (d) were cleaned subsequently with 2.5% HCl, 5% NaOH, acetone and methanol solutions for removal of possible oxide layer and then washed out by distilled water. Iron films of the same thickness 1020 nm were deposited by thermal evaporation using resistively heated tungsten filament sources on samples (a), (b), and (c) heated to 300 $^{\circ}$C at 5 x 10^{-7} Torr. Samples were further sealed in their own quartz ampoules at 10^{-5} Torr and simultaneously annealed at 1000 $^{\circ}$C for 24 days. Sample (d) was not exposed to iron film deposition and was placed in the same ampoule together with sample (c) to evaluate whether iron diffusion occurs only from the solid phase or from the gas phase as well . The gradient measurements of Fe:ZnSe samples exposed to different pre-cleaning treatment were performed by 2.8 μm radiation of Cr co-doped Er:YSGG laser and are depicted in Figure 3-10.

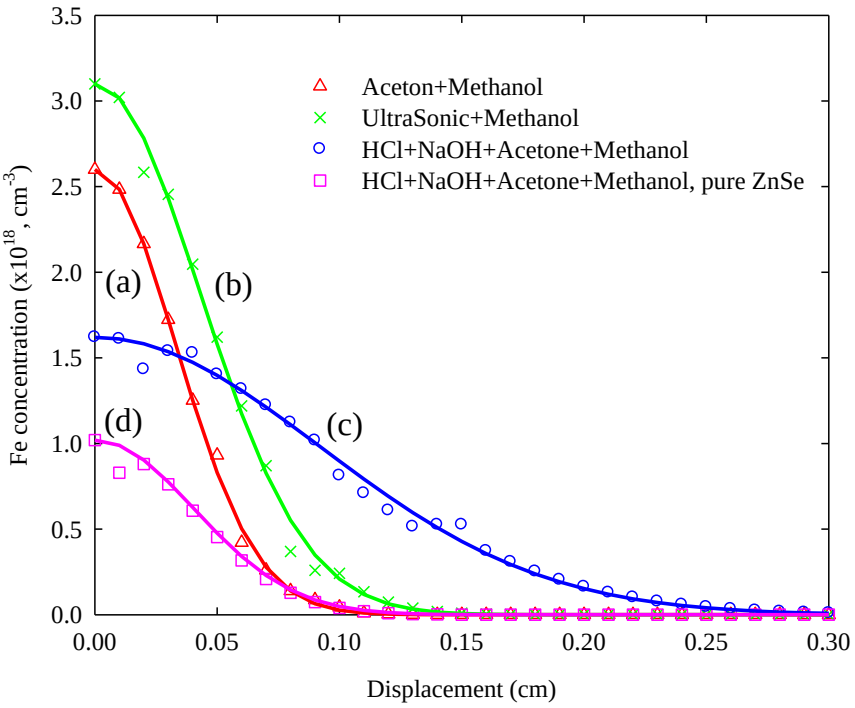

Figure 3-10. Fe^{2+} concentration (experimental points and theoretical fits - solid lines) *vs*. distance from the surface of ZnSe samples exposed to different pre-cleaning treatment.

The results of Fe gradient measurements are summarized in Table 2. After 24 days of thermal diffusion approximately more than a half of iron metal film on the ZnSe surface was diffused in the host crystal. Hence, the process for samples (a), (b), and (c) was treated as diffusion from the source with constant iron concentration. Optimized pre-cleaning of the crystal surface (sample c) removes barriers for iron diffusion and results in 5-6 fold increase of the measured iron coefficient of diffusion. In addition to diffusion from the metal phase, iron also sublimates in ampoule enabling diffusion from the gas phase.

Table 2. Pre-cleaning method and diffusion parameters for Fe:ZnSe polycrystals

	Chemicals	Annealing Time (Days)	Diffusion coefficient ($x10^{-10}$, cm^2/s)	Diffusion length (mm)
Sample (a)	$A^1 + M^2$	24	2.64	0.47
Sample (b)	$U^3 + M$	24	4.47	0.61
Sample (c)	HCl+NaOH+A+M	24	20.4	1.3
Sample (d)		24	3.96	0.57

[1.] Acetone; [2.] Methanol; [3.] Ultrasonic

In addition, the substrate temperature has been varied from 0 to 430 ℃ for the cohesion and homogeneity of Fe on ZnSe while using the same surface pre-cleaning recipe (2.5% HCl, 5% NaOH, acetone and methanol). Five identical samples with 2 μm Fe film thickness deposited only on one surface of ZnSe crystal were annealed at 1000 ℃ during 564 hours to estimate the diffusion parameters of Fe in ZnSe. The transverse dimension for all samples was 6.29x6.23 mm^2 with a thickness 4.13mm and they were cut to 6.29x4.13 mm^2 with a thickness 1.5 mm. The 4 mm thick sample was sufficient to avoid the influence of Fe diffusion from the gas phase through the opposite side of crystal surface for a given annealing conditions. The room temperature absorption measurement

(by Shimadzu UV-VIS-NIR-3101PC and Bruker "Tensor-27" FTIR spectrophotometers) of the annealed samples was carried out to confirm the corresponding $^5E \rightarrow {}^5T_2$ vibronic transition of Fe^{2+} ions as well as an average Fe concentration in ZnSe. Iron distribution in the annealed crystal as a function of substrate temperature was measured using a pulsed Er:Cr:YSGG operating in free running regime with a 2.78 μm radiation as shown in Figure 3-11 (the detailed fitting method is shown in section 3-3-2). Laser radiation was focused into a spot with ~130 μm beam diameter. To avoid absorption saturation, the pulse energy was reduced to the level below the saturation energy of Fe optical centers. The sample with Fe deposited on the unheated substrate is not shown in the Figure 3-11e. Due to the quick oxidation of the film and poor adhesion of Fe film it was easily peeled off.

Table 3 shows the detailed results for five samples with 2 μm iron film annealed at 1000 ℃ for 564 hours. The substrate temperature of 350 ℃ showed an enhanced diffusion coefficient and diffusion length, 1.71×10^{-9} cm^2/s and 1.2 mm, respectively. As the temperature increases, the values of diffusion coefficient and diffusion length were decreased. It can be explained by sublimation of the ZnSe at temperatures around 400 ℃ and possible repelling of the iron ions during the deposition process. The maximum diffusion coefficient and length were estimated as 2.1×10^{-9} cm^2/s and 1.3mm, respectively. The measured diffusion coefficient was ~2.5 times bigger than that calculated from the vapor phase diffusion experiments early reported in [72]. We believe that this difference is due to ZnSe surface pre-cleaning, substrate temperature optimization, and elimination of surface chemical barriers hampering Fe diffusion.

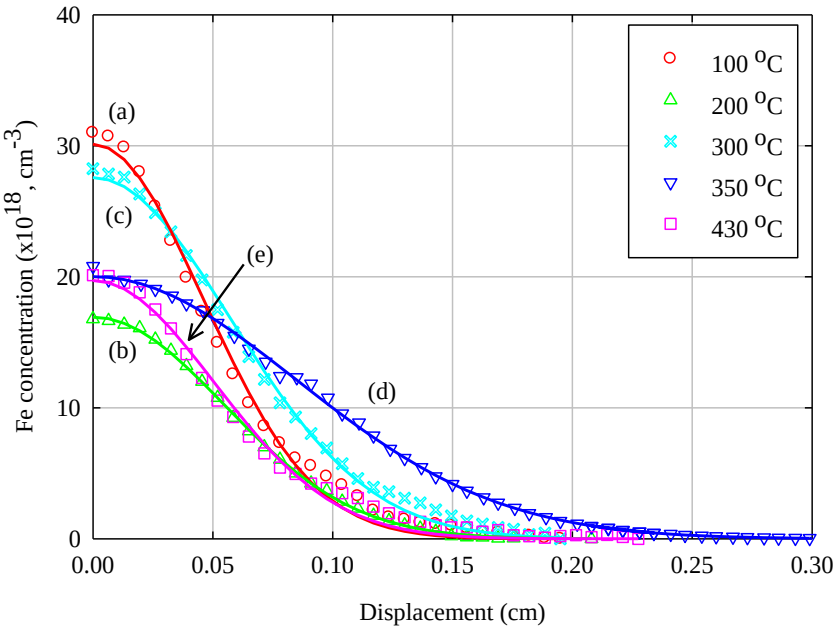

Figure 3-11. Diffusion parameter calculations in terms of substrate temperature; experiments (dots) and fitting (solid); substrate annealing temperature at (a) 100 ℃, (b) 200 ℃, (c) 300 ℃, (d) 350 ℃ and (e) 430 ℃.

Table 3. Diffusion parameters of iron in ZnSe with 2 μm deposited Fe film annealed at 1000 ℃ for 564 hours.

	Substrate Temperature (K)	Diffusion coefficient ($x10^{-10}$, cm^2/s)	Diffusion length (mm)
Sample (a)	100	5.21	0.65
Sample (b)	200	7.34	0.77
Sample (c)	300	8.12	0.82
Sample (d)	350	17.1	1.20
Sample (e)	430	6.28	0.71

Using Fe^{2+} ion concentration in terms of displacement data for the thin film geometry case, the diffusion coefficient for Fe^{2+}:ZnSe from eq. (3-5) and diffusion length by least squares fitting procedure by the computer program (Mathematica 6.0) have been determined as shown in Figure 3-12.

Sample of Figure 3-12A was annealed for 564 hrs at 1000 ℃ and fitting of experimental data results in diffusion coefficient $D = 2.1x10^{-9}$ cm^2/s, and diffusion length of 1.3mm. The diffusion parameters for three different samples with identical Fe films and annealed at the same conditions were very close to each other and varied over the range $1.97\text{-}2.1x10^{-9}$ cm^2/s. Sample of Figure 3-12B was annealed for 420 hrs at T=1000 ℃ and fitting of experimental data resulted in $D=2.24x10^{-9}$ cm^2/s and diffusion length of 1.16mm as shown in Table 4. The measured diffusion coefficient was ~2.5 times bigger than that calculated from the vapor phase diffusion experiments early reported in [72] for diffusion from the gas phase. We believe that this difference is due to ZnSe surface pre-cleaning and elimination of chemical barriers hampering Fe diffusion. It is noteworthy that in our initial experiments of iron thermal diffusion from the metal phase without careful cleaning of the sample surfaces the iron diffusion length was more than 3 times smaller than what was obtained from Figure 3-12.

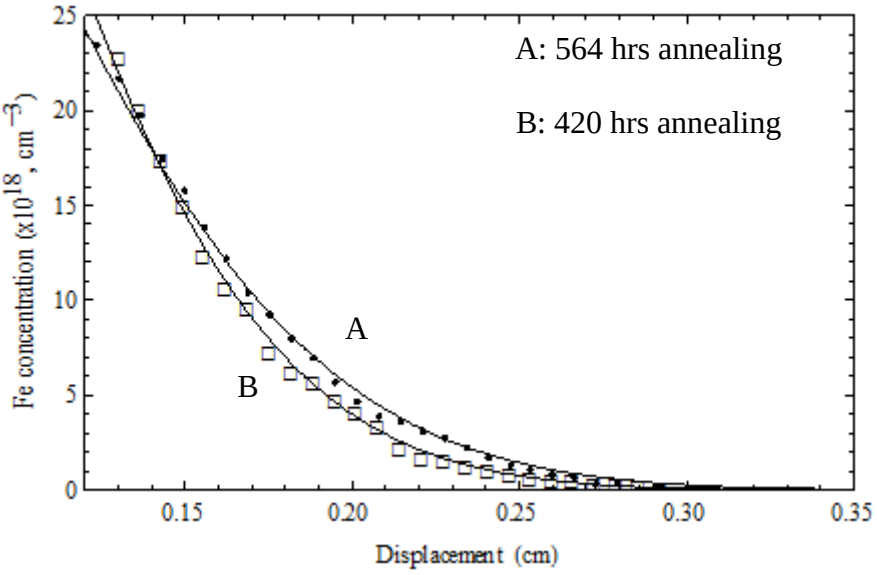

Figure 3-12. Diffusion coefficient calculations by Mathematica for experimental (*dots*) and fitted (*solid*) data.

Table 4. Annealing conditions and diffusion parameters for Fe:ZnSe

Sample	Annealing Time (hrs)	Annealing Temperature (℃)	Diffusion Coefficient ($x10^{-9}$, cm^2/s)	Diffusion Length (mm)
1	564	1000	2.1	1.3
2	564	1000	2.01	1.28
3	564	1000	1.97	1.27
4	420	1000	2.24	1.16

Based on these measurements, three new samples were prepared with different Fe concentrations to calculate the activation energy of diffusion process. The samples were annealed at 950℃ for 564 hrs as sample 1-3 in Table 4. The calculated diffusion coefficient was D=10.3x10^{-11} cm^2/s. Once the diffusion coefficient *D(T)* is determined, the activation energy of diffusion can be determined from the following expression,

$$D(T) = D_0 \exp\left(-\frac{E_{ad}}{K_B T}\right) \tag{3-12}$$

, where D_0 is diffusion coefficient for $1/T \approx 0$, E_{ad} is the activation energy, K_B is Boltzmann constant (1.38x10^{-23} J/K ≈ 0.695cm^{-1}/K), and T is the annealing temperature. Using two different diffusion coefficients (10.3x10^{-11} and 2.1x10^{-9} cm^2/s) at two different annealing temperatures (900 and 950 ℃), the activation energy E_{ad} was estimated as 1.75x10^4 cm^{-1}.

Based on the diffusion parameters that were obtained from the experiments (D=2.1x10^{-9} cm^2/s, and annealing temperature at 950 ℃), the diffusion time and diffusion length could be easily estimated for future reference in Figure 3-13.

3.4 Summary

Thermal diffusion of iron in the ZnSe and ZnS crystals was studied and optimized. The special treatment of the crystal surfaces before iron film deposition allows us to increase thermal diffusion coefficient by a factor of 10 in comparison with a simple cleaning procedure using acetone and methanol. From the temperature dependence of the diffusion coefficient in the ZnSe crystals, the activation energy E_{ad} was estimated as 1.75x10^4 cm^{-1}. Developed technology allows us to fabricate large highly doped (up to

C_{Fe}=112×10^{18} cm^{-3}) laser elements with *cross-section* area 3x3mm^2 and uniform iron distribution.

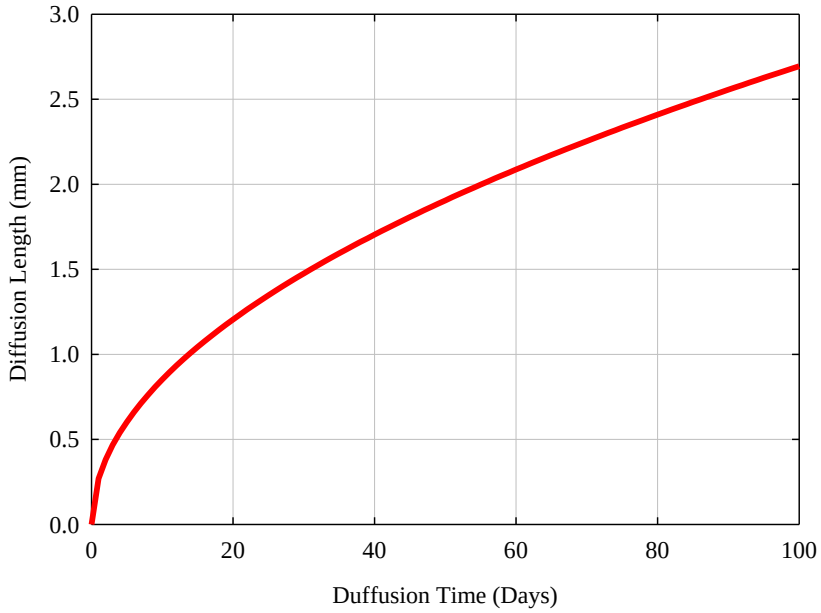

Figure 3-13. Estimated diffusion length *vs*. annealing time for *D*=2.1x10^{-9} cm^2/s diffusion coefficient and 1000℃ annealing temperature.

CHAPTER 4

OPTICAL CHARACTERIZATION OF Fe^{2+}:ZnSe AND ZnS CRYSTALS

The developed crystals have been characterized in terms of absorption, emission spectra, and kinetics of luminescence at different temperatures. Cross-sections of emission, absorption and concentration quenching thresholds were identified. The absorption spectra for all samples were measured using Shimadzu UV-VIS-NIR-3101PC and Bruker 'Tensor-27' FTIR spectrophotometers to confirm the corresponding $^5E \rightarrow {}^5T_2$ vibronic transition of Fe^{2+} ions as well as an average Fe concentration in ZnSe.

4.1 Mid-IR absorption & emission spectra of Fe^{2+}:ZnSe and Fe^{2+}:ZnS

The energy structure of TM ions in II-VI semiconductors has been extensively studied since 60s [73]. Prior to the optical characterization, it is important to take a look at the crystal field splitting. If an atom is considered by itself, the five *d* orbital orientations (d_{xx}, d_{xz}, d_{yz}, $d_x{}^2{}_{-y}{}^2$, and $d_z{}^2$) have the same energy associated with them. They are said to be degenerate, meaning that each orbital has the same energy. However, if an outside field is brought near the atom, the orientations of the different *d* orbitals cause them to act differently from one another. This is what happens to metallic ion placed within a node of the host crystal lattice. The electrons from other atoms surrounding the metal atom cause its *d* orbitals to split in energy domain. The orbitals oriented towards the other atoms have a higher energy. This splitting of the orbitals is called *crystal field splitting*. The type of a node the metal atoms occupies determines how

the *d* orbitals split. The ^5D ground state of Fe^{2+} ($3d^6$) in the tetrahedral crystal field (T_d) of ZnSe crystal is split into the doublet ^5E and triplet $^5T_2$. In tetrahedral symmetry, the overall optical transition ($^5E \rightarrow {}^5T_2$) is both electric and magnetic-dipole allowed [74].

Absorption band corresponds to the $^5E \rightarrow {}^5T_2$ vibronic transition in iron ions. It is easy to determine the absorption cross section ($\sigma_{Fe}{}^{2+}$) and concentrations of the Fe^{2+} after the values of the absorption coefficients were obtained. Similar to Cr^{2+}($3d^4$) ions, the ground and first excited levels of Fe^{2+}($3d^6$) ions have the same spin, and therefore will have a relatively high cross-section of emission. However, unlike Cr^{2+}ions [75], the absorption band of the Fe ions in chalcogenides is not described by a Gaussian profile as shown in Figure 4-1.

The room temperature absorption spectra were recorded for all samples in the 300-3200 nm spectral range using Shimadzu UV-VIS-NIR-3101PC and in the 2.2-10 μm spectral range using Bruker "Tensor-27" FTIR spectrophotometers. The spectral resolution of the spectrophotometer was set to 0.8 nm. Figure 4.1 demonstrates the active absorption spectra (Fresnel losses were subtracted) which were converted from the transmission spectra for Fe doped ZnSe in the wavelength range 0.2-6μm.

The samples were annealed with different film thicknesses (30, 60, 140, 200, 450 nm of sandwich geometry) at the same temperature (1000 ℃) for 17 days annealing as shown in Table 5. The iron concentrations in ZnSe host crystals were estimated with an absorption cross-section ($\sigma=0.85 \times 10^{-18}$ cm^{-2}) at 2.8 μm at 300K. The absorption band positioned between 2.2 and 5.8 μm and originating from the ^5E ground state was used to estimate the value for the Fe^{2+} concentration.

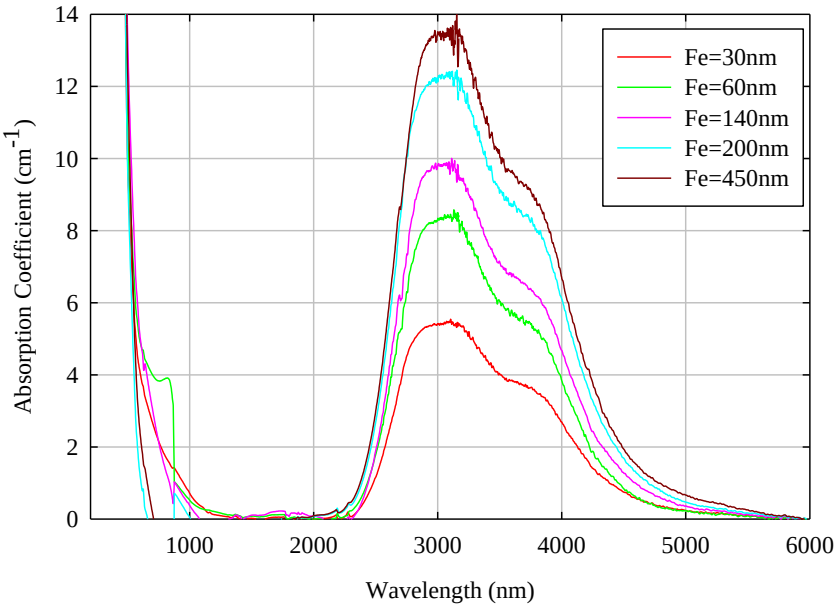

Figure 4-1. Absorption spectra of Fe:ZnSe in terms of Fe film thickness at 300K.

Table 5. Fe concentration dependence on transmission and absorption coefficient (α) (σ=0.85x10^{-18} cm^{-2} at 2.8 μm) in ZnSe at 300K.

Fe film thickness (nm)	Concentration (x10^{18}, atoms/cm^3)	Transmission ($T_{2.8\mu m}$, %)	Absorption coefficient ($\alpha_{2.8\mu m}$ cm^{-1})
30	2.44	55.59	4.89
60	4.52	42.35	7.16
140	9.74	36.14	8.48
200	13.91	27.29	10.82
450	31.31	25.78	11.30

This wide absorption band of Fe:ZnSe allows the use of Er:Cr:YSGG laser operating at 2.8 μm as a pump source. The peak intensity of absorption scales linearly with the Fe concentration.

The room temperature absorption spectra for Fe:ZnS polycrystals were recorded for all samples in the 300-3200 nm spectral range using Shimadzu UV-VIS-NIR-3101PC and in the 2.2-10 μm spectral range using Bruker "Tensor-27" FTIR spectrophotometers. The spectral resolution of the spectrophotometer was set to 0.8nm. Figure 4.2 describes room temperature active absorption band (Fresnel losses were subtracted) between 2 and 4.8μm corresponding to ^5E ground state for Fe doped ZnS polycrystals. The samples are annealed with different iron concentration (Fe=1-23x10^{18} cm^{-3}) with sandwich geometry at the same temperature (950 ℃) for 30 days annealing. The iron concentrations in ZnS host crystals were estimated with an absorption cross-section ($\sigma \approx 1x10^{-18}$ cm^2 [76]) at 2.8 μm at 300K. The wide absorption band over 2-4.8 μm of Fe:ZnS also allows the use of Er:Cr:YSGG laser operating at 2.8 μm as a pump source.

The fluorescence spectra of $^5T_2 \rightarrow {}^5E$ steady-state at various temperatures were measured for different Fe concentrations. The emission characterization of the Fe^{2+}:ZnSe crystals has been studied by direct excitation with the 2.8 μm radiation of Er:Cr:YSGG laser. For the low temperature, doped samples were placed in a close-cycle helium cryostat and the fluorescence spectra were measured with a computer-controlled Acton Research 'ARC-300i' spectrometer and liquid nitrogen cooled InSb detector (Teledyne Judson J10D-M204-R250) equipped with 'Perry Amplifier' which provides a 10 *ns* (10/90%) rise time and DC to 50 MHz response trans-impedance.

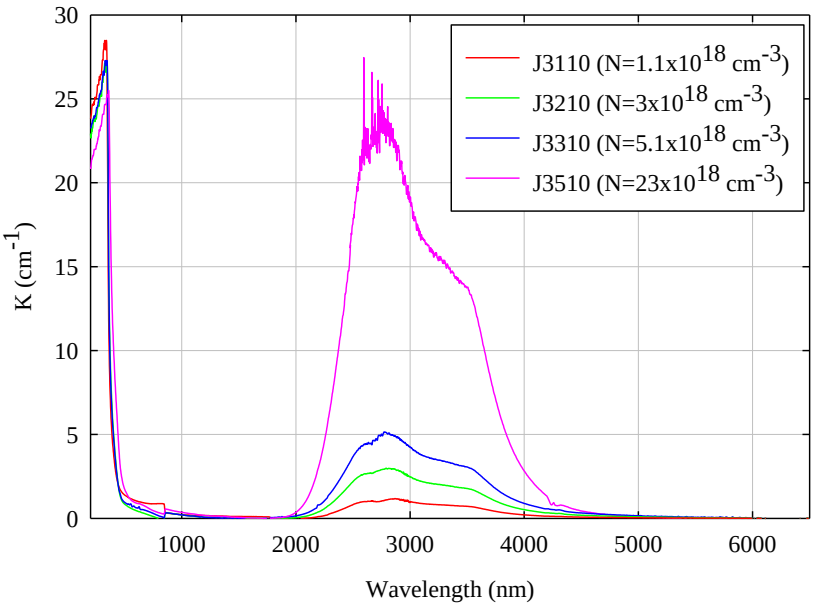

Figure 4-2. Absorption spectra of Fe:ZnS at 300K.

The PL emissions from Fe doped ZnSe samples were measured at different temperatures (14-250 K) over the spectral range from 3200 to 5200 nm. The temperature dependent luminescence measurements corresponding to $^5T_2 \rightarrow {}^5E$ transition of Fe^{2+} ions in ZnSe measured for two different concentrations of the lowest Fe concentration, $6x10^{18}$ cm^{-3} and the highly Fe doped sample, $112x10^{18}$ cm^{-3} are depicted in Figure 4.3 and Figure 4.4, respectively. As temperature increases, the intensity of Fe luminescence in ZnSe decreases meaning that the temperature quenching occurs for all Fe concentrations. The line shape broadens as the temperature increases. CO_2 absorption takes place at 4.2 μm as indicated in the figures.

We have monitored the effect of iron doping in ZnS on the photoluminescence intensity at 3-5μm wavelength range. The intensity of luminescence slightly increases with the iron concentration increase from 1 to $5x10^{18}$ cm^{-3}. But the intensity slightly drops at highly Fe doped ZnS (Fe=$23x10^{18}$ cm^{-3}) which is not significant. Figure 4.5 and 4.6 show the temperature dependence of luminescence of Fe:ZnS with the Fe concentration varying over 1-$23x10^{18}$ cm^{-3} at 14 and 300K, respectively. At 14K, there are three narrow bands at 3.4, 3.45, and 3.5 μm, however, these bands disappeared at 300K while the kinks still remain between 3.3 and 3.4μm. At 300K, CO_2 absorption still appears at 4.2 μm. Therefore, the concentration quenching is not important for Fe:ZnS.

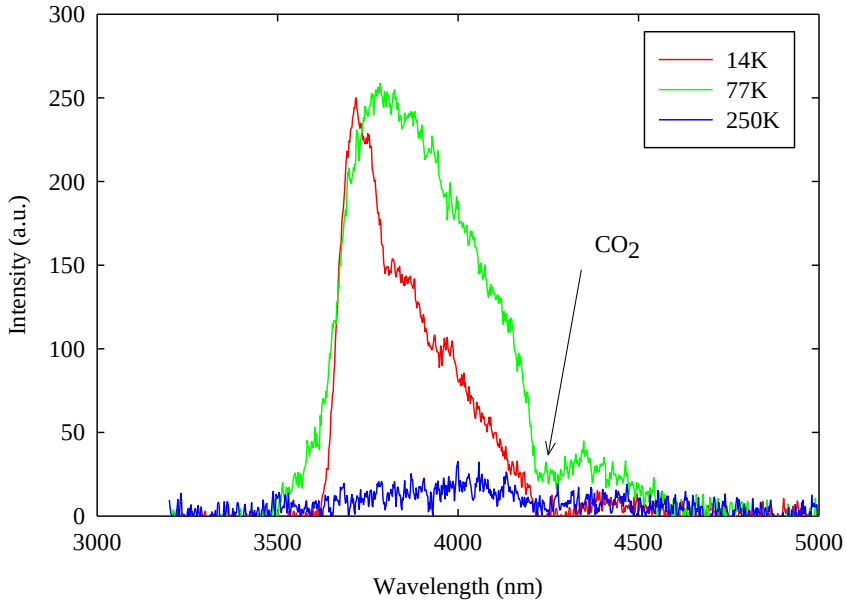

Figure 4-3. Temperature dependence of $^5T_2 \rightarrow {}^5E$ luminescence of Fe^{2+} ions in ZnSe for low (5.8×10^{18} cm^{-3}) Fe concentration.

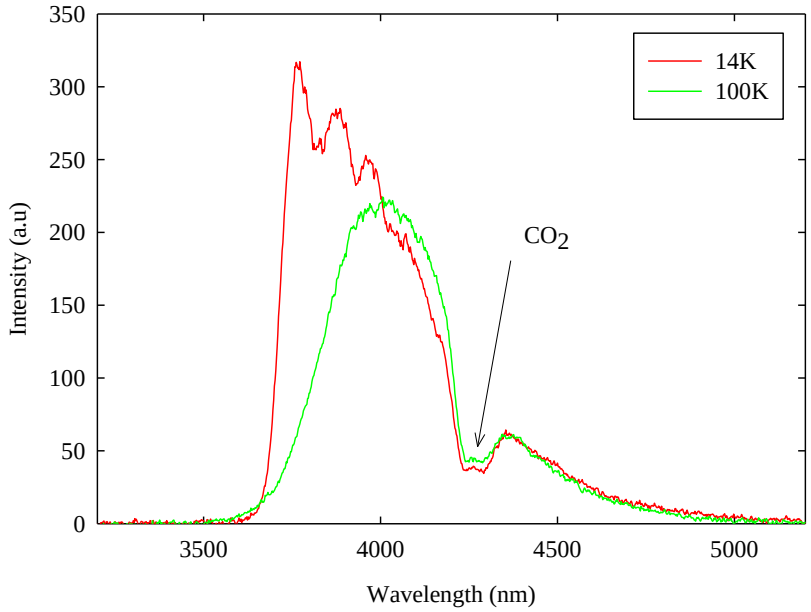

Figure 4-4. Temperature dependence of $^5T_2 \rightarrow {}^5E$ luminescence of Fe^{2+} ions in ZnSe for high (112×10^{18} cm^{-3}) Fe concentration.

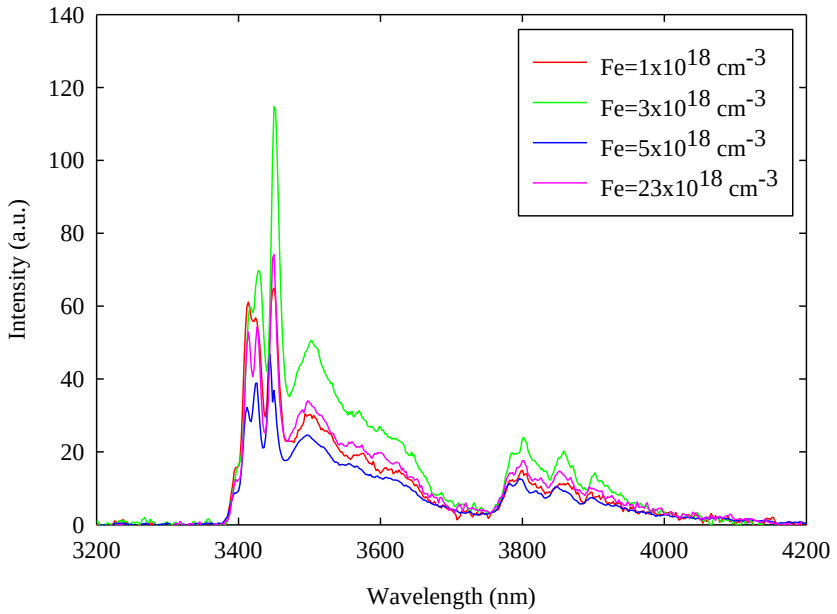

Figure 4-5. Concentration dependence of $^5T_2 \rightarrow {}^5E$ luminescence of Fe^{2+} ions in ZnS measured at 14 K.

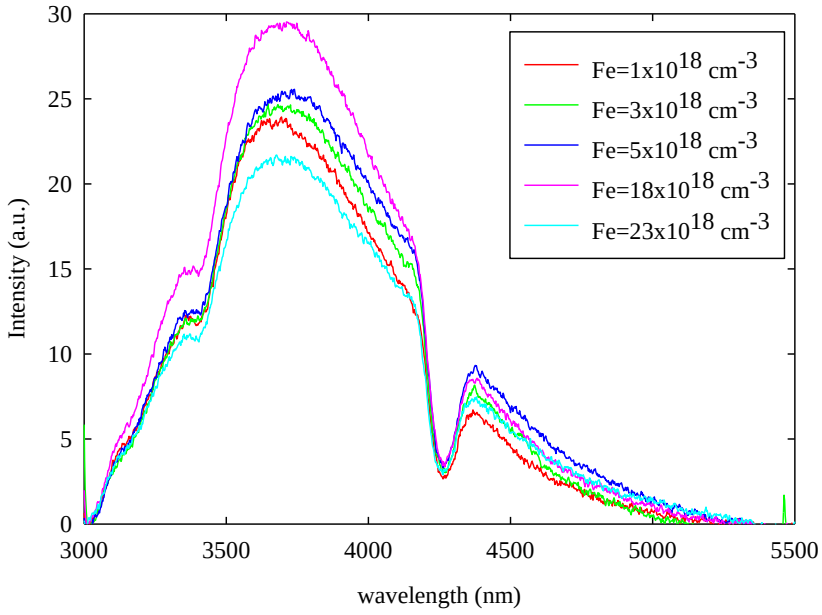

Figure 4-6. Concentration dependence of $^5T_2 \rightarrow {}^5E$ luminescence of Fe^{2+} ions in ZnS measured at 300 K.

4.2 Kinetics of luminescence of Fe:ZnSe crystals

The information from a steady-state scan with fluorescence intensity versus wavelength represents the averaged behavior of what occurs during the entire scan. Luminescence itself, however, occurs on the micro-nanosecond timescale. Therefore, if snapshots are taken at nanosecond speed, much more information about the mechanisms of impurity ion relaxation in a host crystal can be revealed. This is the reason why measurements of kinetics of luminescence of optical centers are so important. In this paragraph, the kinetics behavior of Fe optical centers will be studied as a function of Fe concentration and crystal temperature. There are two complementary techniques of kinetics of luminescence measurement: the time domain and the frequency domain.

In the time domain, a short pulse laser radiation excites the doped samples, and the subsequent fluorescence emission is recorded as a function of time with a nanosecond timescale. In the frequency domain, a given sample is excited by a modulated laser source. The fluorescence emitted by the sample has a similar waveform, but it is modulated and phase-shifted from the excitation regime. Both the time and wavelength domain measurements use the fluorescence decay law. A given sample is excited with a pulsed laser. The width of the pulse is made much shorter than the decay time τ of the sample. The time dependent intensity is measured following the excitation pulse, and the decay time τ is calculated from the slope of a plot of *log I(t)* versus *t*, or from the time at which the intensity decreases to *1/e* of the intensity as shown in Figure 4.7. Suppose a sample is excited with an infinitely sharp (δ-function) pulse of light. This results in an initial population (n_0) of the sample in the excited state. The excited state population decays with a rate $\Gamma+k_{nr}$ according to

$$\frac{dn(t)}{dt} = (\Gamma + k_{non-rad}) \cdot n(\mathrm{t})\,, \tag{4.1}$$

where *n(t)* is the number of excited centers at time *t* following excitation, Γ is the spontaneous emission rate, and k_{nr} is the non-radiative decay rate. Since emission takes place randomly and each excited molecule has the same probability of emission in a given period of time, it results in an exponential decay of the excited state population, $n(t)=n_0 exp(-t/\tau)$.

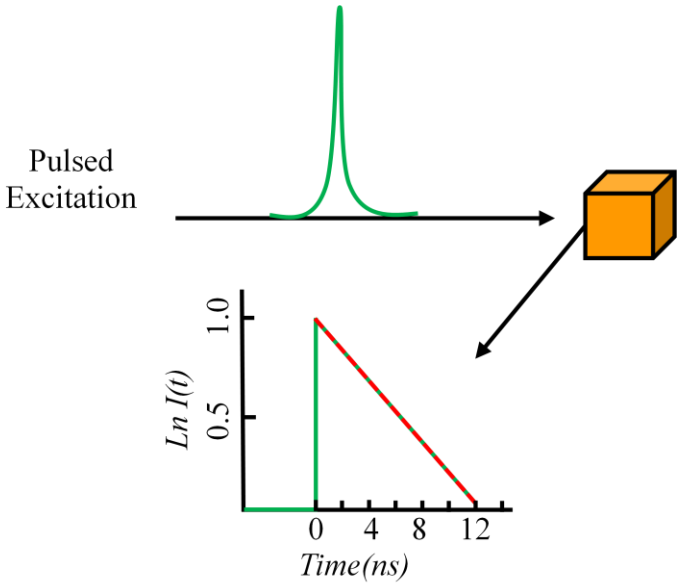

Figure 4-7. Schematics for luminescence lifetime measurement.

In luminescence experiments, the number of excited optical centers may not be observed, but rather luminescence intensity which is proportional to *n(t)*. Hence, eq.4-1.can be written in terms of the time dependent intensity *I*(*t*) as follows

$$I(t) = I_0 \exp\left(-\frac{t}{\tau}\right), \tag{4.2}$$

where I_0 is the intensity at time=0. The lifetime τ is the inverse of the total decay rate, $\tau=(\Gamma+k_{nr})^{-1}$. In general, the inverse of the lifetime is the sum of the rates which depopulate

the excited state. The lifetime is the average amount of time the optical center remains in the excited state following excitation.

In these experiments, the kinetics of mid-IR luminescence of Fe:ZnSe (or Fe:ZnS) under direct excitation with a 2.8 μm radiation of passively Q-switched Cr co-doped Er:YSGG laser were recorded for low ($0.1x10^{18}$) and high ($112x10^{18}$ ions/cm^{-3}) concentrations at different temperatures. A flash-lamp pumped Er:Cr:YSGG laser at 2.8μm wavelength was equipped with electro-optic Pockels cell ($LiNbO_3$) and featured 80 *ns* pulse duration in Q-switch regime of operation. The electro-optic Pockels cell is equipped with +24 VDC power and minimum 10 *ns* (maximum 1 μs) pulse width. The samples were placed in closed cycle refrigerator at vacuumed to less than $3x10^{-6}$ Torr. The temperature dependence of lifetime was taken for sample temperatures varying from 14 to 300 K using 3-5.5 μm band-pass filter in front of the optical detector. A liquid nitrogen cooled InSb (Indium Antimonide) and HgCdTe (Mercury Cadmium Telluride) detectors with a 3 μm filter were used for non-selective PL as well as for kinetics of luminescence measurements as shown in Figure 4.8. However, since both detectors have slower response time at high temperature in comparison to the lifetime of Fe:ZnSe first excited level, for the accurate lifetime measurement at temperatures above 250 K, fast response time detector is required.

Figure 4.9 shows Fe:ZnSe polycrystals with sandwich geometry Fe deposition. The light color (yellowish one) represents lowest Fe concentration and the dark color corresponds to the highest Fe concentration.

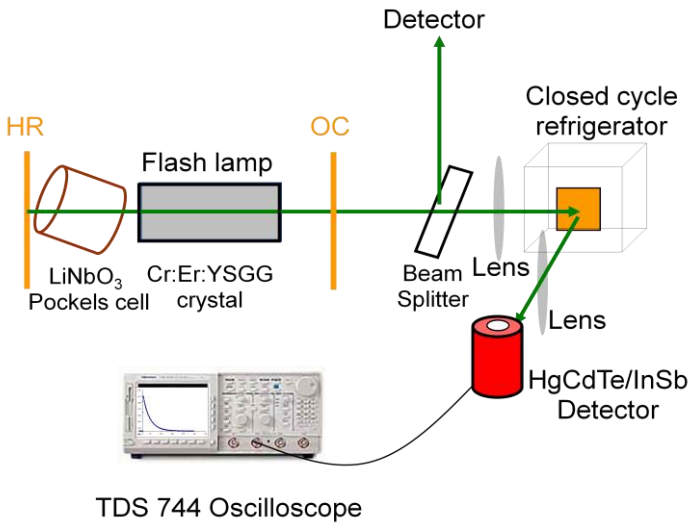

Figure 4-8. Schematics of experimental setup for kinetics of luminescence measurement.

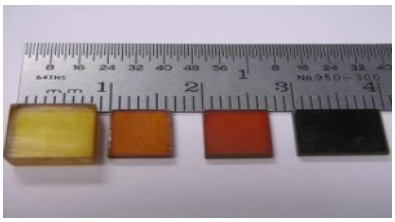

Figure 4-9. Photo of Fe:ZnSe samples with different (increasing from left to right) concentrations of Fe ions.

The luminescence lifetime studies over the 15-300 K temperature range were reported in [14] and [21]. In [21] the Fe:ZnSe single-crystal samples with iron concentration varied from 3.4 to 6.5×10^{19} cm^{-3} were reported. In the temperature range from 12 to 120 K, the lifetime unexpectedly increased from 33 μs to 105 μs and then decreased with temperature due to temperature induced non-radiative process. Similarly, an unusual growth of the luminescence lifetime with temperature increase between 14K and 120 K was reported in [14**Error! Bookmark not defined.**] where it was attributed to the thermal population of iron sub-levels with smaller oscillator strength. In the current study we also observed an increase of the luminescence lifetime with the temperature increase from 14K to 120K in the Fe:ZnSe sample with iron concentration $C_{Fe}=5\times10^{18}$ cm^{-3}. The kinetics of luminescence of this sample at 20 K and 77 K are shown in the Figure 4.10 (curve iii and iv). As one can see from the Figure 4.10 the luminescence decay reveals a single exponential behavior with luminescence lifetimes τ=68 μs at T=77 K and τ=54 μs at T=20 K. However, in the crystal with 85 times smaller iron concentration, $C_{Fe}=0.1\times10^{18}$ cm^{-3}, the kinetics of the luminescence at low temperature were similar to each other over the 14K-110K temperature range with luminescence lifetime ~τ=57±4 μs (see Figure 4.10, curves (i) and (ii)). Therefore, we consider that an unusual increase of lifetime between 14K and 110K reported in the papers [14,21] results from iron-iron interactions and luminescence re-absorption at low temperatures. The highly doped sample ($C_{Fe}=86\times10^{18}$ cm^{-3}) also reveals an asymptotic decay at T=110 K (curve (v)) longer than that at T=20 K (curve (vi)), but low temperature kinetics of this sample were essentially non-exponentials. One of the reasons of the non-exponential behavior could be related to multi-center formation in the highly doped crystals.

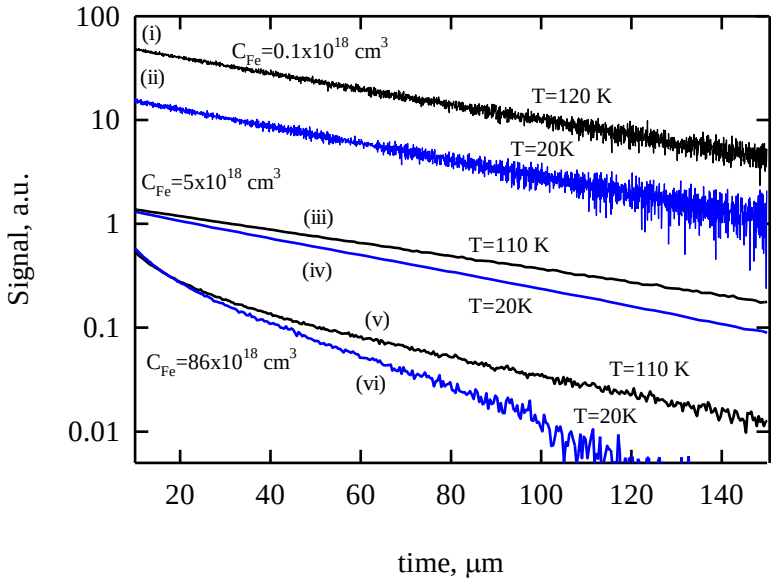

Figure 4-10. Kinetics of luminescence of Fe:ZnSe samples with iron concentration C=0.1×10^{18} cm^{-3} (i,ii); C=5×10^{18} cm^{-3} (ii,iv); and C=86×10^{18} cm^{-3} (v,vi); at T=20K (ii;iv;vi), T=110K (iii,v); and T=120K (i)

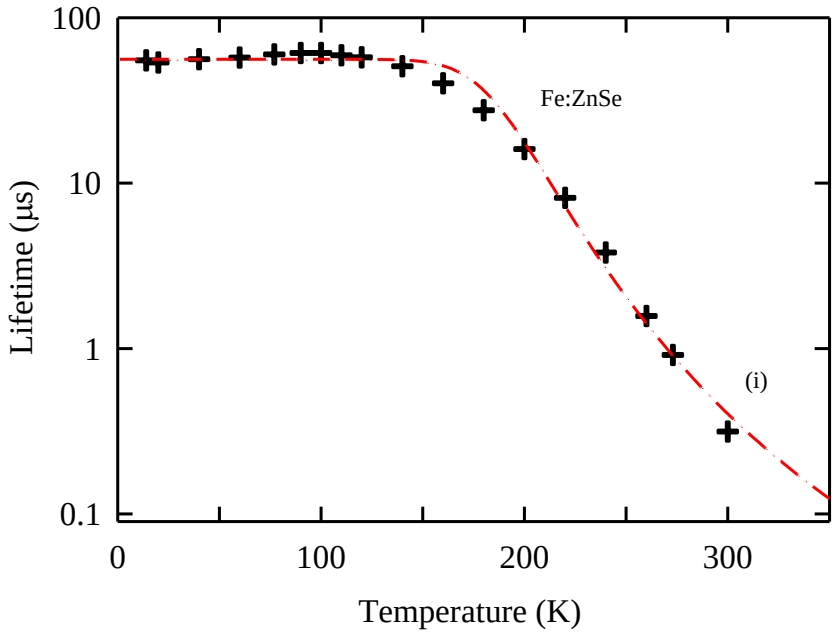

Figure 4-11. Luminescence lifetime *vs*. temperature for Fe:ZnSe (+ - C=0.1×10^{18} cm^{-3})

The temperature dependence of the luminescence lifetime of the low doped (C_{Fe} =0.1×10^{18} cm^{-3}) Fe:ZnSe sample is shown in the Figure 4.11. As it was mentioned above, in the 14-120K temperature range the luminescence lifetime was unchanged with τ=57±4 μs then decreased with temperature, due to the thermally activated non-radiative decay. The experimental data are fit with non-radiative process which describes a model of thermally activated radiationless processes based on intersection of configuration coordinates of the first exited and ground levels. This process is typical for non-radiative relaxation in optical centers with a strong electron-phonon coupling. This approach leads to a temperature dependence of the upper level lifetime given by the following equations (see for example [77]):

$$\tau^{-1}(T) = \tau_{rad}^{-1} + W_{nr} \tag{4.3}$$

$$W_{nr} = W_0 \exp(-\Delta E_a / kT) \tag{4.4}$$

where τ_{rad} - radiative lifetime, W_{nr} -nonradiative relaxation rate, ΔE_a – activation energy which is the energy gap between the intersection of adiabatic potentials of the ground and excited states and the minimum of adiabatic potential of excited state, W_0 -relaxation parameter; and k_B - Boltzmann constant. The best fit yield the parameters of ΔE_a=2500 cm^{-1} and *1/Wa=0.1 ns* (see Figure 4.11, curve i).

The temperature measurements of the low doped sample allow us to estimate the radiation lifetime of the $^5E \leftrightarrow {}^5T_2$ transition as τ_{rad}=57±4 μs. Using this value of the radiative lifetime, the emission cross sections at RT was calculated from *Fuchtbauer–Ladenburg* equation [78] :

$$\sigma_{em}(\lambda) = \frac{\lambda^5 I(\lambda)}{8\pi c n^2 \tau_{rad} \int I(\lambda) \lambda d\lambda}, \tag{4.5}$$

where $\sigma_{em}(\lambda)$ is emission cross section, λ-emission wavelength, n - refractive index, c-speed of light, τ_{rad}- radiative emission life-time, and $I(\lambda)$ -luminescence spectrum measured in energy per area per sec units. The maximum value of the emission cross-section calculated from the above measurements was equal to $\sigma_{em}=1.2\times10^{18}$ cm^2 at 4.3 μm.

Figure 4.12 shows room temperature kinetics of luminescence of the Fe:ZnSe crystal with iron concentration varied from 0.1 to 112 $\times10^{18}$ cm^{-3}. The kinetics of luminescence of the low doped Fe:ZnSe crystal (Figure 4.12, curve 1) was single exponential at RT with luminescence lifetime τ_{RT}=382 *ns*. This decay time is significantly smaller than the radiative lifetime (τ_{rad}) at $^5E\leftrightarrow{}^5T_2$ transition and is determined by a thermally induced non-radiative process. The photoluminescence kinetics of the highly doped crystals reveals a non-exponential decay (Figure 4.12, curve 4). However, asymptotic decay curves were exponential (Fig 4.12.B) with small decrease of the life-time to 309 *ns* for $C_{Fe}=112\times10^{18}$ cm^{-3} iron concentrations in comparison with 382 *ns* for $C_{Fe}=0.1\times10^{18}$ cm^{-3}. The decreases of the asymptotic decay rate of the highly doped crystals in comparison with a low doped crystals as well as non-exponential decay are the characteristic features of the energy migration process. The decay rate (Wq) induced by concentration quenching could be calculated as a difference of the asymptotic decay rates of the low and highly doped samples, but even for highly doped sample Wq=0.6 μs^{-1} is still smaller than temperature quenching of the luminescence. Simulation of photoluminescence decay of the highly doped samples requires a numerical simulation of the energy migration processes including multi-center complexes of the iron in the highly doped crystal (good approximation could be obtained by a double exponential decay fit

with a time constants τ_1=309 *ns* τ_2=138 *ns*). However, it is convenient for laser applications such as passive Q-switching, mode-locking and gain-switched lasing to estimate an average relaxation time $<\tau_{av}>$ defined as $\int I(t)/I_{max}dt$. Figure 4.13 shows a dependence of the average relaxation rate on iron concentration. As one can see from the Figure 4.13, the decay rate decreases from 382 *ns* for low concentrated sample to 186 ns for Fe:ZnSe sample with iron concentration C_{Fe}=112 $\times 10^{18}$ cm^{-3}. The concentration dependence of the average decay time can be fitted by an empirical equation

$$\langle \tau_{av} \rangle = \frac{\tau_r}{1+N_{Fe}/N_0}, \tag{4.6}$$

where, N_{Fe} is the concentration of the Fe^{2+} ions, and N_0 is the critical concentration parameter where decay time is reduced by a factor of 2. The least-squares fit to the experimental lifetime data by using this equation is also shown in Figure 4.13 (dashed curve). The best-fit values of N_0 were determined as 106×10^{18} cm^{-3}. The decay times shown in Figure 4.13 are longer than typical pulse duration of the Q-switched lasers (~100 *ns*) and hence, Fe:ZnSe crystals can lase at room temperature under short-pulse gain-switched excitation.

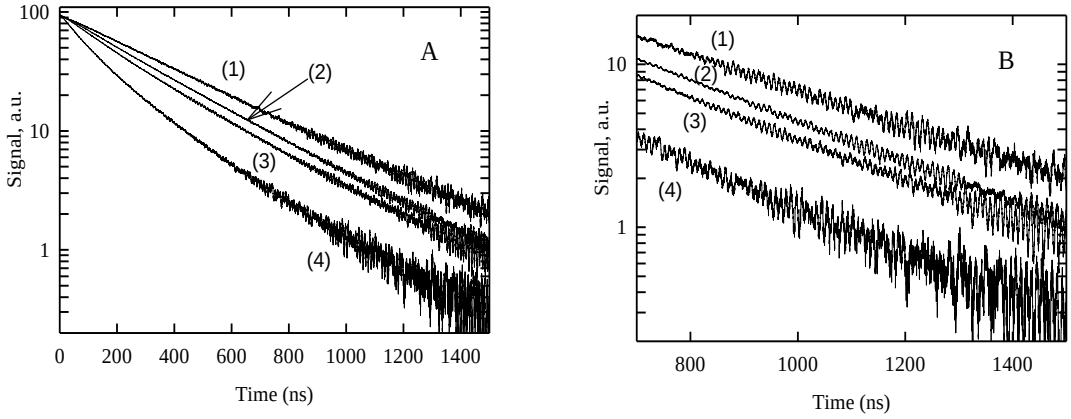

Figure 4.12. A) Kinetics of luminescence of the Fe:ZnSe samples with different iron concentrations: (1) C_{Fe}=0.1 ×10^{18} cm^{-3}; (2)C_{Fe}=14×10^{18} cm^{-3}; (3)C_{Fe}=45×10^{18} cm^{-3}; (4) C_{Fe} =112 ×10^{18} cm^{-3}, *B)* the same kinetics with time scale zoomed in.

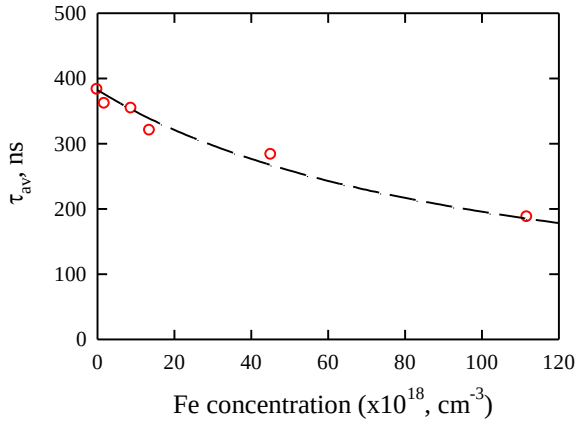

Figure 4.13. Average relaxation time at the $^5T_2 \rightarrow {}^5E$ transition *vs*. iron concentration in Fe:ZnSe samples measured at room temperature (dashed line shows fit using eq. 4.6).

4.3 Kinetics of luminescence of the Fe:ZnS crystals

Zinc Selenide crystal is one of the most frequently used active element host for Cr^{2+} and Fe^{2+} based mid-IR lasers. However iron doped Zinc Sulfide crystal is also very attractive for mid-IR laser applications. First of all, due to a bigger crystal filed splitting of the ^5D ground state the absorption and emission spectra are shifted to the shorter wavelength in comparison with the ZnSe host (see Figures 4.1-4.6). As a result, room temperature luminescence spectra of the Fe:ZnS cover 3-5 μm spectral range. Due to strong absorption bands of hydrocarbons and other organic molecules in this spectral range Fe:ZnS lasers are very promising for sensing applications. In this study, we report temperature dependences of the mid-IR photoluminescence of the Fe:ZnS samples with iron concentration varied over 1-23x10^{18} cm^{-3} range. Figure 4.14A shows kinetics of luminescence of the Fe:ZnSe crystals measured at T=220 K with three different iron concentrations. All studied kinetics of luminescence were exponential with a luminescence lifetime τ=182 *ns* for all studied samples. Due to the limitation of pumping source pulse duration (80 *ns*), the lifetime of the Fe:ZnS samples could not be obtained at temperatures above 250 K, where temperature quenched Fe:ZnS lifetime becomes comparable with the pump pulse duration. Decreasing crystal temperature to 14K results in monotonous increasing of the luminescence lifetime to τ=6.2 μs and 5.5 μs for iron concentration C_{Fe}=1x10^{18} cm^{-3} and C_{Fe}=23x10^{18} cm^{-3}, correspondingly (see Figure 4.15). The temperature dependence of the luminescence can't be fitted by a thermally activated radiationless relaxation model based on single configuration-coordinate. A more accurate model should consider additional physical processes and more accurate energy structure. It is known, that Jahn-Teller interaction results in additional splitting of the upper and

ground state ^5D levels, therefore a more accurate model should include several radiationless processes with different relaxation parameters. The solid curve in the Figure 4.15 shows fitting by two relaxation processes described by eq.(4.4) with parameters: ΔE_{a1}=818 cm^{-1}; $1/W_{01}$=1 *ns*; and ΔE_{a2}=126 cm^{-1} ; $1/W_{02}$=420 *ns*. At high temperatures, the relaxation should also include multi-phonon processes [77]. The more accurate model required additional experimental study of the luminescence lifetime at high temperature with a short pulse excitation. Extrapolation of the luminescence lifetime to room temperature allows us to estimate the lifetime of Fe^{2+} ions in ZnS as τ=50 *ns*.

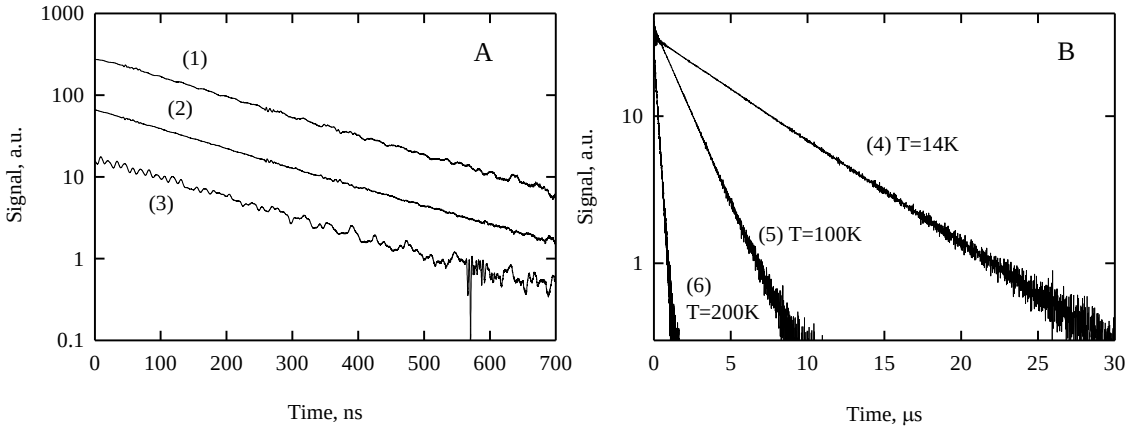

Figure 4-14. A) Kinetics of luminescence of the Fe:ZnS samples with different iron concentrations: (1) $C_{Fe}=1\times10^{18}$ cm^{-3}; (2) $C_{Fe}=5\times10^{18}$ cm^{-3}; (3) $C_{Fe}=23\times10^{18}$ cm^{-3} at T=220K; B) Kinetics of luminescence of Fe:ZnS for $C_{Fe}=1x10^{18}$ cm^{-3} at different temperatures (4) T=14K; (5) T=100K; (6) T=200K

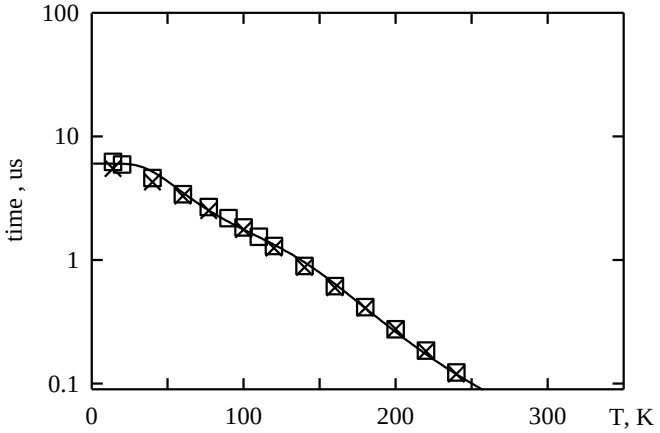

Figure 4-15. Luminescence lifetime *vs.* temperature for Fe:ZnS crystals (×:$C_{Fe}=1\times10^{18}$ cm^{-3} and □:$C_{Fe}=23\times10^{18}$ cm^{-3})

4.4 Optical characterization of Co:Fe:ZnSe crystals

Since the TM ions exhibit broad absorption and emission bands with large oscillator strengths in the Mid-IR regimes as shown earlier, absorption and emission bands can be superimposed with appropriate choice of co-dopants. Hence, they will provide possible energy transfer paths between the different ions and enable a new pump schemes by producing a desired emission when direct pump sources are not available. For example, energy transfer between Fe^{2+} and Ni^{2+} in ZnSe was reported in [79]. The photoluminescence band exhibiting fine structure with no-phonon line at 1178 cm^{-1} was detected in Ni:ZnSe crystals which was interpreted as a $^3T_1(P) \rightarrow {}^3T_1(F)$ transition in a tetrahedral crystal field.

Various excited state processes play a crucial role in the laser performance. The quenching of luminescence reduces the excited state lifetime and can cause sample heating, therefore inducing photo-thermal effects such as thermal lensing and thermal shock. Luminescence quenching also results in reduced laser slope efficiency. Other excited state processes that require consideration are excited state absorption and energy transfer. In excited state absorption a photon excites an electronic center from the ground state to an excited sate, which then relaxes to some lower lying metastable level. A second photon promotes the center to an even higher energy state. Energy transfer takes places when the optical centers are close enough to interact and when the concentration exceeds some lower bound, which is not necessary to be large concentration. Although the energy levels of the interacting ions can be unaffected at such concentrations, the inter-ion interaction is strong enough to enable excitation to be transferred between them. The information of energy transfer are readily studied through the luminescence channel

of the optical pumping cycle, including the concentration, excitation and time dependences of the up-converted luminescence spectra.

The simplest method of transferring excitation from one ion to another involves the absorption of the photon emitted by the excited donor (Co^{2+}) at the acceptor site (Fe^{2+}). This process of radiative energy transfer may be repeated many times before a photon emitted by the donor exits the crystal. In general, energy transfer is non-radiative and the emission-reabsorption mechanism is replaced by site-to-site transfer mediated by some inter-ionic coupling mechanism.

The non-radiative energy transfer process in Figure 4.16 is associated with the simultaneous de-excitation of the donor ion and excitation of the acceptor by an electrostatic, magnetic or exchange coupling between them. A distinguishing feature associated with non-radiative energy transfer is a decrease in donor ion's emission decay time.

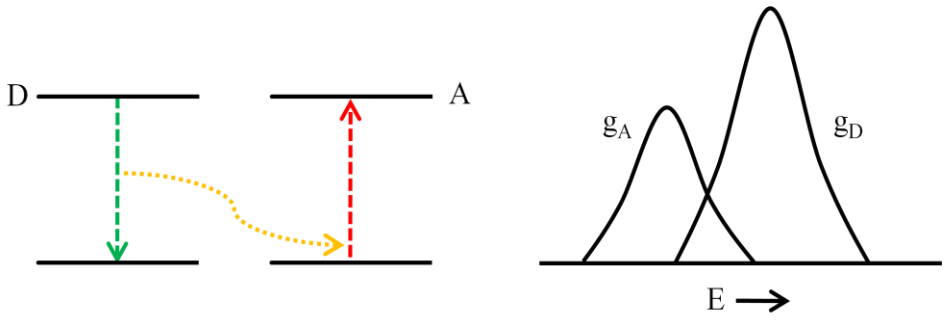

Figure 4-16. Energy transfer between excited donor and acceptor; the ions have the same electronic energy level structure with overlap of emission and absorption band, required by conservation of energy.

The energy transfer rate between donor and acceptor is well explained by Forster-Dexter theory [80] as

$$W_{\mathrm{DA}} = \frac{2\pi}{\hbar} |< D, \mathrm{A}^{*} | \mathrm{H}' | \mathrm{D}^{*}, \mathrm{A} >|^{2} g_D(E) g_A(E) dE, \qquad (4.7)$$

where normalized shape of function $g_D(E)$ and $g_A(E)$ for homogeneously broadened, radiative emission ($g_D(E)$) and absorption ($g_A(E)$) transitions on donor ($D^* \rightarrow D$) and acceptor ($A \rightarrow A^*$), respectively. There are three interactions that could be extracted from this equation by expanding the electrostatic interaction term between electrons on the donor and acceptor, H′ such as electric dipole-dipole term, electric dipole-quadrupole term and electric quadrupole-quadrupole that are related to the donor-acceptor separation [81]. Assuming allowed electric dipole and electric quadrupole transitions for the matrix elements appropriate to radiative transition leads to the energy transfer by electric quadrupole system can be significant in solids although the radiative electric quadrupole transition is minute.

Energy transfer due to an unintentional co-dopant may change the characteristics of a desired transition, such as the pumping efficiency and emission lifetime of a particular ion. Lately, some research on absorption, photoluminescence (PL), and time resolved PL measurements due to energy transfer between Co^{2+} and Fe^{2+} ion in diffusion-doped ZnSe [82] stimulate us to try Co^{2+} co-doping of Fe^{2+}:ZnSe crystals.

Two types of TM ions doped in II-VI semiconductors were prepared for optical characterization: Fe and Co doped ZnSe and ZnS polycrystals. We hypothesize that due to Co-Fe energy transfer, Co:Fe:ZnSe crystals could be pumped with a convenient alexandrite (740 nm) and/or Er:YAG (1645 nm) excitations. To characterize the efficiency of Co-Fe energy transfer the kinetics of luminescence measurements have been performed as a function of Fe and Co concentration using 1.55μm pump laser based on D_2 1^{st} Stokes shifting of 1.06 μm Nd:YAG laser radiation and optical parametric oscillator operating at 1.55μm with 10 *ns* pulse duration.

A controlled thermal diffusion of the iron ions was used to fabricate co-doped Co:Fe:ZnSe and Co:Fe:ZnS samples with Fe concentration range of 8.5-19x10^{18} cm^{-3}, and 0.5-10x10^{18} cm^{-3}, respectively while cobalt concentration was maintained as 7x10^{18} cm^{-3} for both crystals. Optical parametric oscillator operating at 1.55μm with 10 *ns* pulse duration was used for the direct Co^{2+} ion excitation and the study of the $Co^{2+} \rightarrow Fe^{2+}$ energy transfer process.

Co^{2+} ($3d^7$) in ZnSe and ZnS crystals with a dimension of 10x10x1.2 mm^3 was first diffused for 1 week and Fe thin film was deposited on both crystals using TE method and diffused for additional 2 weeks. Absorption spectra were taken for all samples.

First, for all given lattice constant, the tetrahedral site results in crystal field splitting four-ninths of the corresponding octahedral system. The tetrahedral site in the chalcogenides provides higher oscillator strength for the 3*d*-3*d* transitions of the ions than does an octahedral site. The energy-level diagram of Co^{2+} ($3d^7$) and Fe^{2+} ($3d^6$) in tetrahedral sites is depicted in Figure 4-17. The ground level 4*F* of a free ion Co^{2+} is split into three levels, $^4T_1$, $^4T_2$ and $^4A_2$, by the crystal field. The absorption band transition 1.3–2μm corresponds to $^4A_2$ to $^4T_1$ transition and 0.7μm absorption band from 4*F* ($^4A_2$) to 4*P* ($^4T_1$) transition. The lowest energy transition in the mid-IR band, $^4A_2$ to $^4T_2$ at 3μm, is symmetry forbidden resulting in low cross-section values in absorption and emission which is reported as σ=6x10^{-20} cm^2 [83]. The magnitude of the ^5E to $^5T_2$ splitting for Fe^{2+} in a tetrahedral configuration is estimated to be about 3400 cm^{-1}. The only spin allowed transitions occur between the ^5E and $^5T_2$ levels.

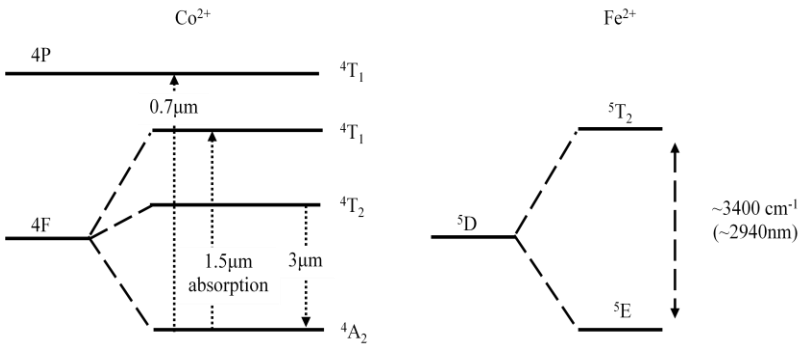

Figure 4-17. Energy level diagram of Co^{2+} ($3d^7$) and Fe^{2+} ($3d^6$) in tetrahedrally coordinated hosts

Absorption and luminescence spectra of the Co:ZnSe (Co:ZnS) and Co:Fe:ZnSe (Co:Fe:ZnS) samples are shown in Figures 4.18 and 4.19. Mid-IR luminescence band of the Co^{2+} ions well overlaps with absorption spectrum of the iron ions. Figures 4.18 and 4.19 demonstrate luminescence band of Co:Fe:ZnSe and Co:Fe:ZnS samples under excitation into Co^{2+} ions absorption band at 1.5 μm. Luminescence spectra of the Co:ZnSe and Co:ZnS samples were also measured for comparison. These Figures show a strong evidence of the $Co^{2+} \rightarrow Fe^{2+}$ energy transfer process resulting in the 3-5 μm luminescence of the Fe^{2+} ions. In this experiment we used a low-pass filter with wavelength cut-off at 3μm to avoid the second order of diffraction in the spectrometer. This filter cuts the photoluminescence signal of Co^{2+} ions below 3 μm.

According to the earlier report [82], the energy transfer rate is expected to decrease with respect to the temperature in general. However, the broadening is negligible compared to the bandwidth, and a temperature-independent transfer probability should be expected. On the other hands, if the sample temperature is high enough, the broadening rate of the linewidth with temperature becomes smaller, and then the transfer probability will be independent with temperature.

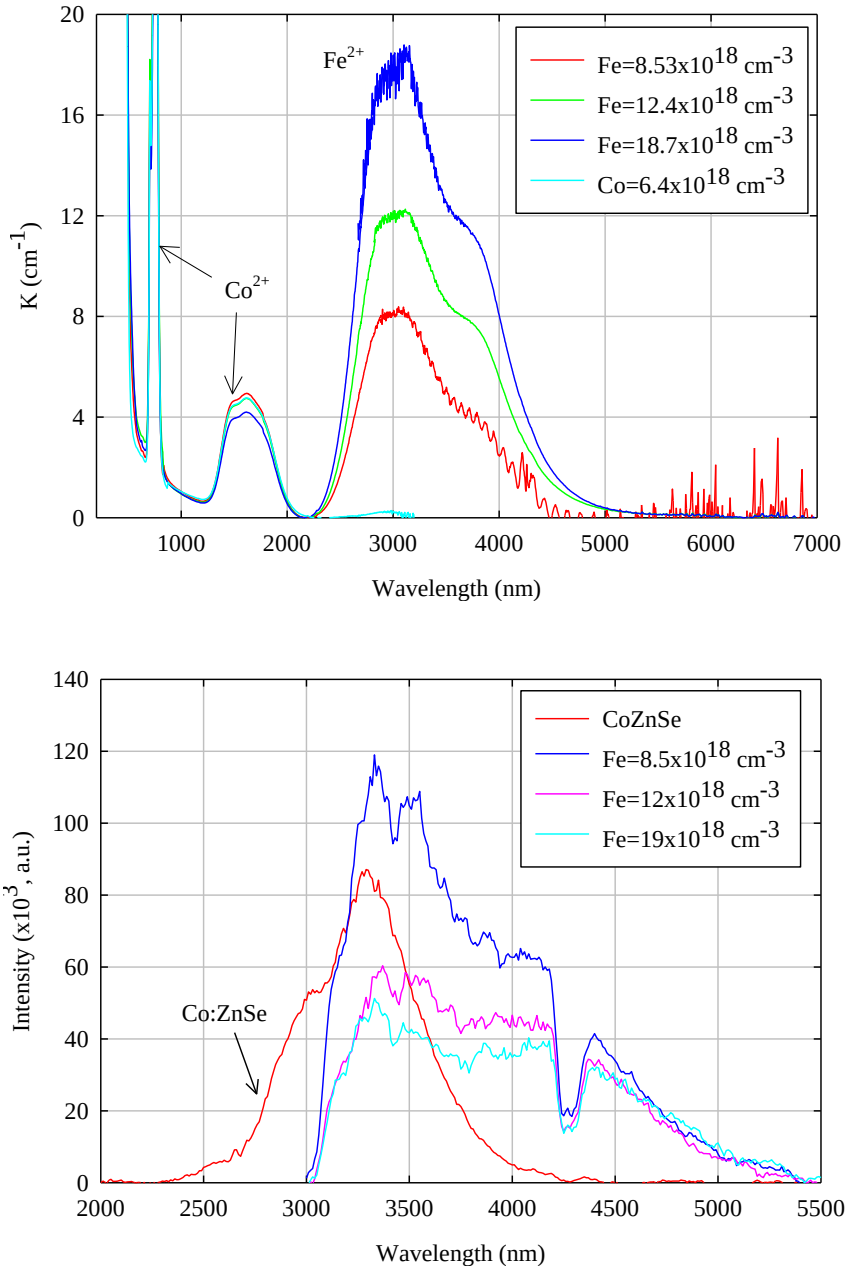

Figure 4-18. Absorption (top) and luminescence (bottom) spectra for cobalt co-doped Fe:ZnSe; Co^{2+} concentration is fixed at $6.4x10^{18}$ cm^{-3} for all samples at 300K; Fe concentration varies over $8.5\text{-}19x10^{18}$ cm^{-3}; 3μm pass-filter used for luminescence spectra

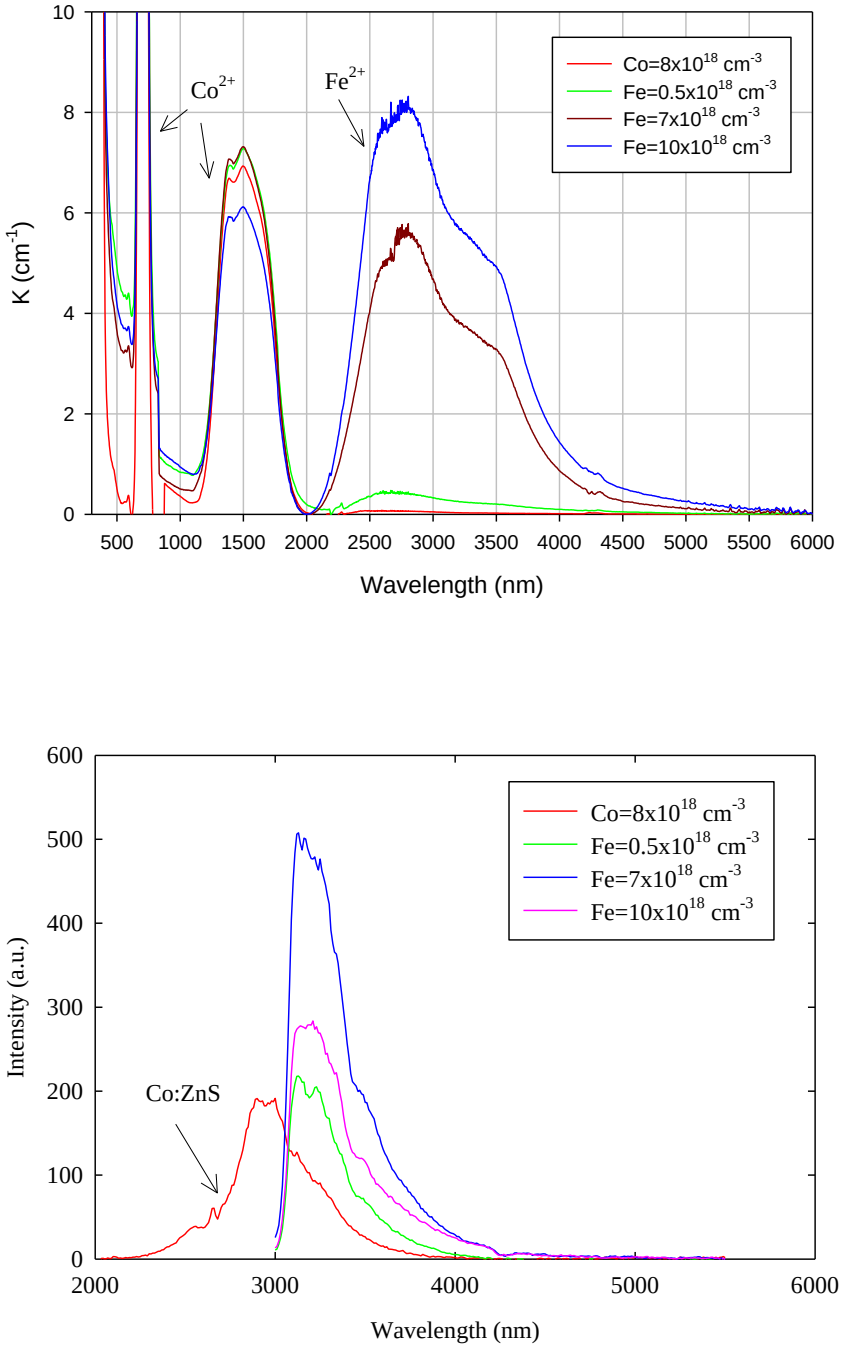

Figure 4-19. Absorption (top) and luminescence (bottom) spectra for cobalt co-doped Fe:ZnS; Co^{2+} concentration is fixed at $8x10^{18}$ cm^{-3} for all samples at 300K; Fe concentration varies over 0.5-$10x10^{18}$ cm^{-3}.

The kinetics of luminescence of Co^{2+} photoluminescence signal featured a decrease of the decay time due to energy transfer to iron ions. In Figure 4-20(A), kinetics of luminescence for Co:ZnSe was taken as a function of temperature. As temperature increases, the lifetime slightly increases up to 100 K. And then it decreases dramatically at higher temperature. These results for Co:ZnSe are similar to the data reported in [7]. As iron is introduced into ZnSe, the strong excitation of Fe^{2+} via Co^{2+} channel in ZnSe was observed. As we observed earlier, the emission from Co^{2+} and absorption from Fe^{2+} are well overlapped over all temperatures. For the lifetime fitting, luminescence decays for Co:ZnSe revealed a non-single exponential. However, all iron doped Co:ZnSe showed single exponential decays (see Figure 4.20) except for 300 K. As temperature increases, lifetime of Fe^{2+} excited by Co^{2+} increases up to 100 K due to thermally activated non-radiative decay, and then it starts decreasing. In Figure 4-20 (D), the kinetics of luminescence for Co:Fe:ZnSe at 4500 nm with 3 μm pass-filter in terms of temperature variations were analyzed. The luminescence decays were fit with single exponential at this wavelength in the range of Fe concentration from $8.5\text{-}19\text{x}10^{18}$ cm^{-3}.

Temperature dependent kinetics of luminescence of cobalt co-doped Fe:ZnS crystals were recorded at fixed wavelengths: for Figure 4-21 (A) Co:ZnS at 2860 nm, (B) Fe:Co:ZnS for $N_{Fe}=0.5\text{x}10^{18}$ cm^{-3}, (C) Fe:Co:ZnSe for $N_{Fe}=7\text{x}10^{18}$ cm^{-3}, and Fe:Co:ZnS for $N_{Fe}=10\text{x}10^{18}$ cm^{-3} at 3010 nm.

In Figure 4.22, the temperature dependence of kinetics of luminescence for Fe:Co:ZnS has been measured at (A) 3010 nm and (B) at 4500 nm. The behavior of lifetime in terms of temperature was similar to Fe:ZnS. However, due to a long lifetime

of cobalt in II-VI semiconductors, the overall lifetime of Fe^{2+} in ZnS boosts up above 200μs at 300 K unlike Fe:ZnS (90μs at 220 K).

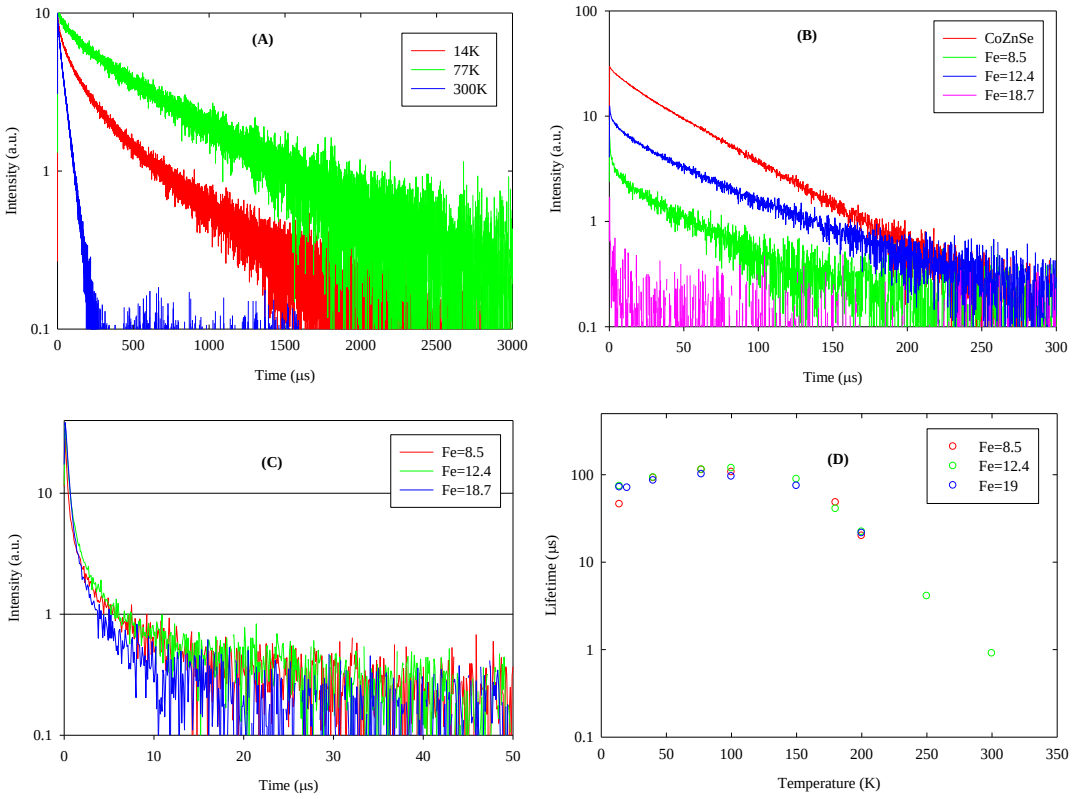

Figure 4-20. Temperature dependence of kinetics of luminescence for (A) Co:ZnSe at 3050nm; (B) Co:ZnSe and Fe:Co:ZnSe at 3050nm at 300K; (C) Fe:Co:ZnSe at 4500nm at 300K; (D) at 4500nm with 3μm pass-filter in terms of temperature variations; luminescence decays were fit with single exponential at this wavelength; Fe concentration varies from 8.5 to $19x10^{18}$ cm^{-3}.

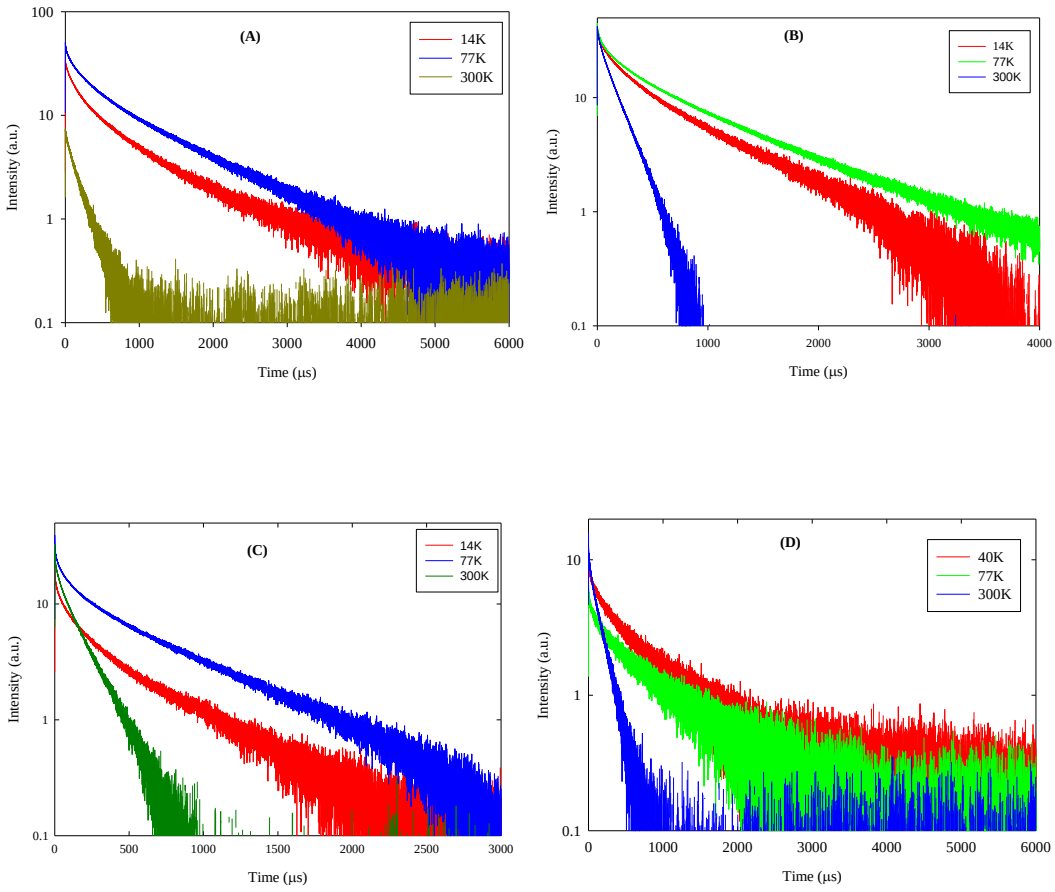

Figure 4-21. Temperature dependence of kinetics of luminescence for (A) Co:ZnS at 2860nm; Fe:Co:ZnS (B) Fe=0.5x10^{18} cm^{-3} (C) Fe=7x10^{18} cm^{-3} (D) Fe=10x10^{18} cm^{-3} at 3010nm.

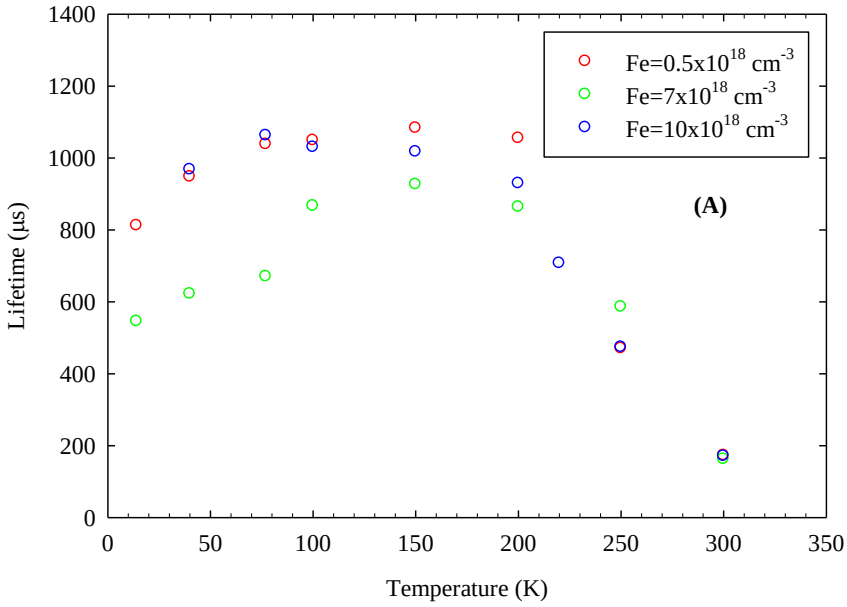

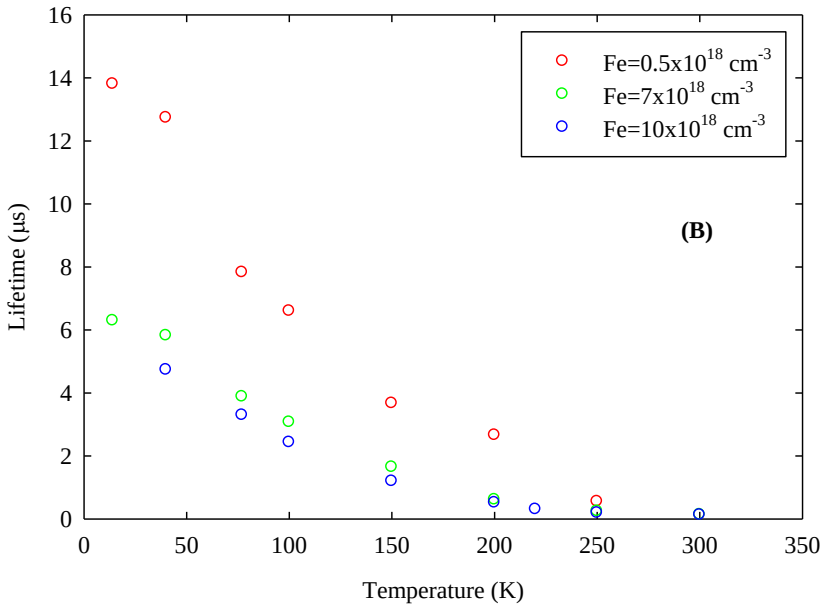

Figure 4-22. Temperature dependence of kinetics of luminescence of Fe:Co:ZnS; (A) at 3010 nm and (B) at 4500 nm

4.5 Summary

1. Concentration dependences of the mid-IR kinetic of luminescence at ${}^5E \leftrightarrow {}^5T_2$ transition in Fe:ZnSe and Fe:ZnS laser samples were studied over 14K-300K temperature range. Radiation lifetime in Fe:ZnSe samples measured using low doped samples with iron concentration 0.1×10^{18} cm^{-3} was estimated to be 57μs.
2. Room temperature maximum emission cross section was calculated to be $\sigma_{em}=1.2\times10^{18}$ cm^2 using *Fuchtbauer–Ladenburg* equation.
3. The luminescence lifetime of the Fe^{2+} ions in the ZnS samples is thermally quenched even at T=14K. The room temperature luminescence lifetime in the Fe:ZnS crystals estimated from the temperature dependence was equal to 50*ns.*
4. The energy transfer to Fe^{2+} (${}^5T_2$) ions under the Co^{2+} excitation at ${}^4A_1 \leftrightarrow {}^4T_1$ transition at 1.56 μm was investigated. It opens a new pathway for mid-IR Fe^{2+} lasing with the use of readily available commercial pump lasers operating at 1550 and 1645 nm.

CHAPTER 5

MID-IR GAIN SWITCHED Fe^{2+}:II-VI LASERS

5.1 Energy scaling of 4.3 μm room temperature Fe:ZnSe laser

Optimization of the diffusion process and spectroscopic characterization of the iron doped ZnSe and ZnS crystal described in the previous chapters allowed us to fabricate laser gain elements for scaling-up of the output energy of the Fe:ZnSe lasers.

5.1.1 Design 2.78μm pump laser based on actively or passively Q-Switched Er:Cr:YSGG laser radiation

Electro-optical Q-Switching with $LiNbO_3$ Pockels Cells, has been successfully used in a variety of configurations, allowing output energy as high as 24mJ with 80*ns* pulse duration from a flash lamp pumped Er:Cr:YSGG laser operating at 2.78μm wavelength and depicted in Figure 5-1. The electro-optic Pockels cell is equipped with +24 VDC power and minimum 10*ns* (maximum 1μs) pulse width. The experimental setup consists of a 100% high reflection mirror (HR) and 82% reflective output coupler (OC). The HR was placed 69 mm from the end of the Er:Cr:YSGG laser crystal, and the OC was placed 53 mm from the laser crystal.

Input power was determined by directly measuring the voltage across the flash-lamp terminals and then calculating the energy delivered to the flash-lamp via discharge of 18μF capacitor used in the laser power supply. The output energy of the pump source

was measured by two “OPHIR 3A-SH” laser thermal power sensors (D1 & D2) and converted to energy by dividing the power by the repetition rate of the laser. The output energy calibration for Er:Cr:YSGG laser was performed in terms of pump energy and three different pulse repetitions which are 6.67, 7, and 10Hz. The cavity used HR and OC mirrors and contains a laser rod and an electro-optic Q-switch. HR is a dielectric mirror with a reflectivity of 100%. For output coupling mirror different plane-parallel plates were used with a maximum reflectivity that varies from 20% to 70%.

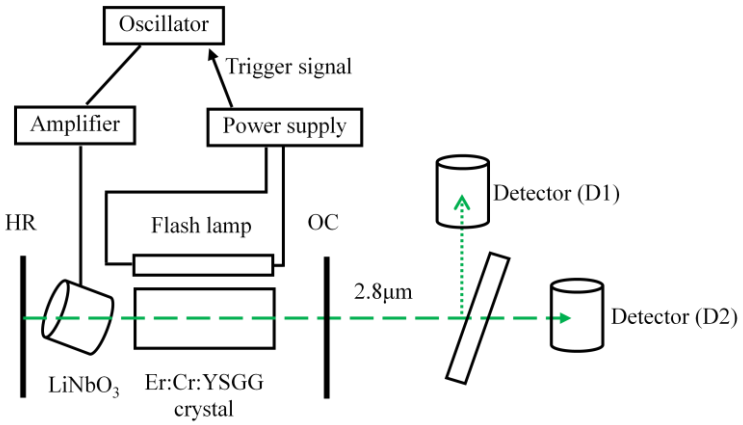

Figure 5-1. Schematic experimental setup of Er:Cr:YSGG laser.

The efficiency of the Q switch regime of operation was approximately 60%, 25% and 22% for 6.67Hz, 7Hz and 10Hz, respectively as shown in Figure 5-2. The major disadvantages of electro-optic switching are the high voltages that are involved, which have to be switched rapidly, producing high electromagnetic noise and pulse instability.

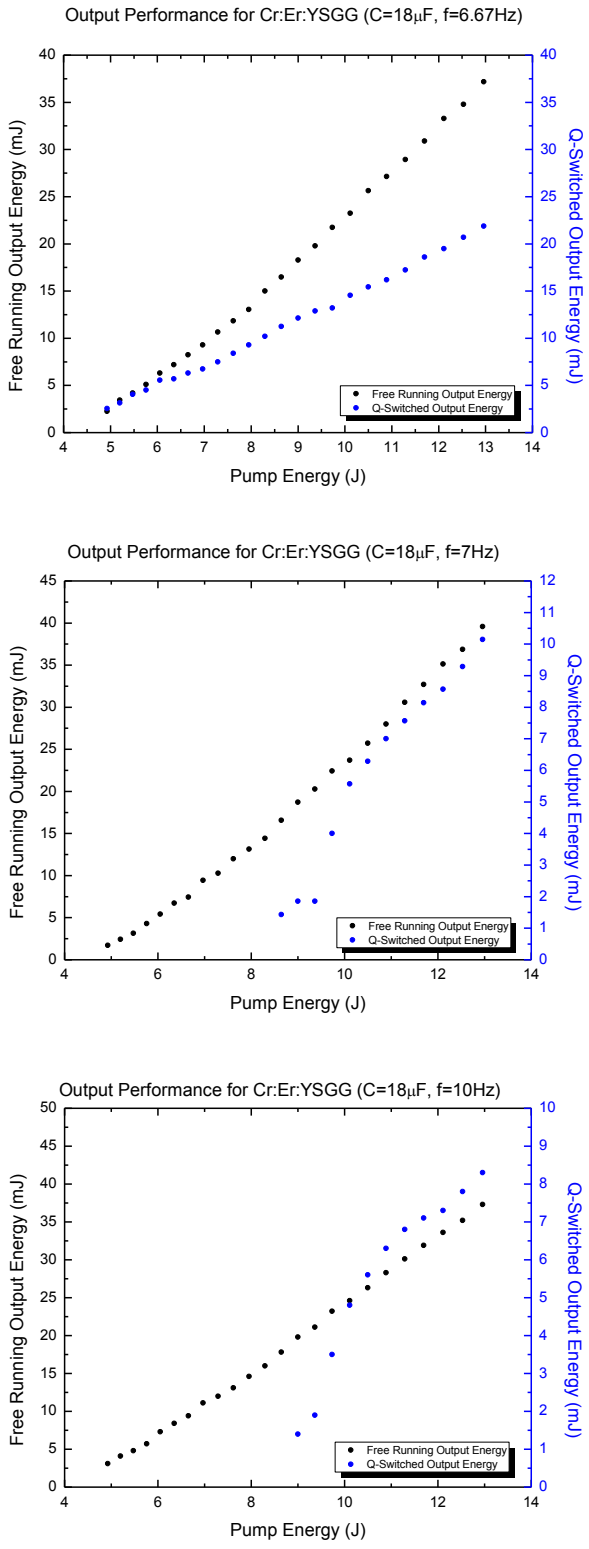

Figure 5-2. Input and output energy for Er:Cr:YSGG for different repetition rates of operation.

5.1.2 High energy Fe:ZnSe gain switched laser

Novel solid state lasers based on transition-metal (TM) doped II-VI semiconductors (Cr^{2+}:ZnSe and Cr^{2+}:ZnS) have been of high interest due to their broad tunability over 1.9-3.3 μm spectral range at room temperature, high optical efficiencies and potential to be scaled to high (>10W) powers via direct fiber or diode pumping [84, 85]. Recent progress has been also undertaken on Fe^{2+} doped II-VI crystals [14,86,87] promising for tunability of mid-IR lasing over 3.5-6 μm spectral range at room temperature. Low temperature lasing of Fe:ZnSe crystals was achieved over 15-180 K temperature range [21]. A continuous-wave oscillation of Fe:ZnSe laser at liquid-nitrogen temperature was reported in [88]. The first room temperature Fe:ZnSe lasing in gain-switched operation mode with tuning over the 3.9-4.8 μm spectral range was demonstrated in [23]. However, the maximum documented single-pulse energy in the gain-switched regime of operation with *ns* pulse durations has been only several hundreds of μJ for many years [47,25]. Fe^{2+}:ZnSe laser energy scaling was reported recently in [89,90]. With the use of Fe:ZnSe gain element grown by Bridgman-technique the output energy reached 1.2 mJ level at 4.5 μm and 65 *ns* pulse duration. In our research group, lasing was studied over 236-300K temperature range. In Fabry-Perot cavity with 18% OC reflectivity the maximum output energy reached 4.7 mJ @ 4.3μm and 3.6 mJ @ 4.37μm at 236K and 300K, respectively. The major problem with the output energy scaling-up was in the development of fabrication technology for large-aperture, good optical quality, high optical density Fe:ZnSe gain elements and in a lack of high energy pump sources.

Figure 5-3 shows an optical scheme of the Fe:ZnSe laser. As a pump source, the actively Q-switched flashlamp-pumped Er:Cr:YSGG laser (oscillation wavelength 2.8

μm) similar to reported in [91] was utilized. The maximum output energy of the pump laser was 33 mJ with the 20 *ns* pulse duration at FWHM. The output radiation was linearly polarized in the horizontal plane. The repetition rate of the Er:Cr:YSGG laser was 6.7 Hz. The uncoated rectangular shape polycrystalline Fe:ZnSe gain element with maximum absorption coefficient of 22 cm^{-1} at 3 μm was used in our experiment. A gain-element was placed inside a sealed container on a cold finger cooled by a tandem of two TE elements.

The primary objective of this experiment was focused on the energy scaling of the Fe:ZnSe laser and laser characterization of the fabricated Fe:ZnSe gain material under short (*ns*) pump pulses. For this gain-switched regime of oscillation the temporal overlap between the pump and oscillation pulses is an essential parameter - poor temporal overlap limits the output energy. To maximize gain, reduce oscillation build-up time, improve pump and output pulses temporal overlap, and provide an effective absorption of the pump beam by the saturated gain element a highly-concentrated ($2x10^{19}$ cm^{-3}) Fe:ZnSe crystal was used. Concentration quenching of Fe ions (274 *ns* for $2x10^{19}$ cm^{-3} vs. 380 *ns* for 10^{17} cm^{-3} at 300 K) was not essential for effective lasing because the values of pump duration and build-up time were more than an order of magnitude smaller than the measured lifetime of Fe ions in ZnSe.

In this work our focus was not on specific cavity design but on the maximum value of energy that can be extracted from the crystal. With regards to the laser cavity it was important to satisfy three main conditions. 1) Short cavity round-trip time enabling small oscillation rise-time and overall improvement of the laser efficiency. 2) Maximum energy stored in the gain medium. 3) Low (<10) Fresnel number providing reasonable

diffraction losses and quality of the output beam. Therefore, we limited our research to a simple short-length unstable plane-plane cavity with an active aperture formed in the gain medium by a focused pump beam. Positive feedback was formed by a dichroic high reflection mirror (HR) and Fresnel reflection from the output facet of the Fe:ZnSe crystal (R=17%). The cavity length between HR mirror and output crystal facet was equal to L=6 cm. Due to a good parallelism of the crystal facets the back surface of the gain element formed a coupled cavity with HR mirror and the crystal output facet. However, the effect of reflection from the back surface of the crystal can be neglected in comparison with the HR mirror reflection. The incident pump beam was focused behind the gain medium by a ZnSe lens (f=20 cm). The maximum output energy was realized with 1.3 mm pump beam diameter at the input crystal surface. The resonator Fresnel number was equal to 6.5, which corresponds to: a) the cavity diffraction losses (~1%) significantly smaller than the active losses through the output coupler, and b) five-fold lower TEM_{oo} mode loss than any of the higher order modes [92]. The energy stored in the gain medium can be increased with the increase of the beam size. However, this approach will result in the increase of the resonator Fresnel Number and decline of the output beam quality. To maximize energy stored in the gain medium we used a highly concentrated ($2x10^{19}$ cm^{-3}) Fe:ZnSe medium which total inversion enables maximum accumulated energy of ~5 mJ.

The aluminum housing that contains the Fe:ZnSe crystal is equipped with Ar gas purging to avoid the moisture accumulation on the crystal facets. The output energy of the pump and Fe:ZnSe lasers were measured by “OPHIR” 3A-SH laser thermal power sensors (D1 and D2). To separate the pump and Fe:ZnSe lasing output, we used a

dichroic mirror (M4) with a 100 %, and 1 % reflectivities at oscillation and pump wavelengths, respectively. Laser spectra were measured using Acton Research "SpectraPro-3000" spectrometer with InSb detector.

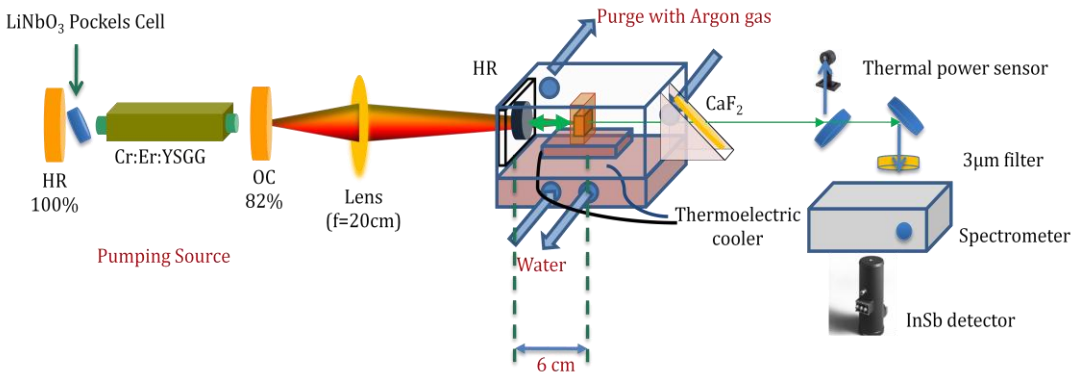

Figure 5-3. Schematics of the Fe:ZnSe laser setup

The output-input characteristics of the Fe:ZnSe laser were studied at different temperatures ranging from 236 K to 300 K. The laser output-input dependences are depicted in Figure 4-4. The following laser slope efficiencies with respect to input pump energy and laser threshold values were measured for different crystal temperatures: 18.9 % and 8.06 mJ at 236 K, 16.6 % and 8.06 mJ at 250 K, 16.6 % and 8.06 mJ at 273 K, and 15.7 % and 9.55 mJ at 300 K, respectively. As one can see, the laser threshold was approximately the same for all studied temperatures and corresponded to the energy density of 4 mJ/cm^2. We found a small increase of the slope efficiency from 16 % to 19 % when crystals temperature was decreased from 300 K to 236 K. This insignificant change in the slope efficiency indicates that temperature quenching of the Fe inversion does not play important role for nanosecond gain-switched regime of oscillation. The maximum measured output energy of the Fe:ZnSe laser was equal to 4.7 mJ and was

limited only by available pump energy. Figure 5-5 indicates that the energy performance of Fe:ZnSe laser slowly decreases as temperature increase.

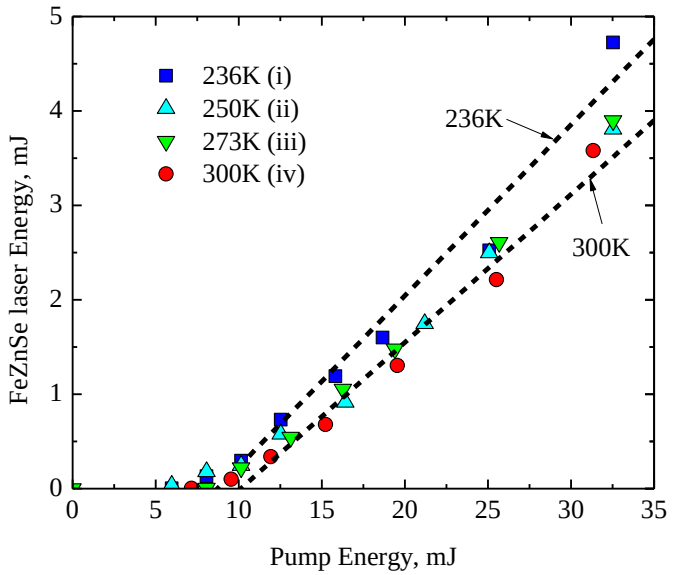

Figure 5-4. Output energy of the Fe:ZnSe laser *vs*. pump energy at 236K (i); 250K (ii); 273 K (iii); and 300 K (iv) temperatures.

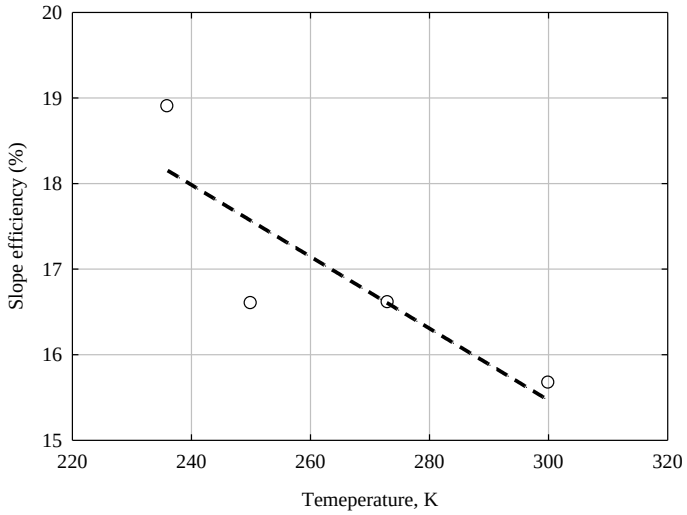

Figure 5-5. Slope efficiency for Fe:ZnSe laser in terms of temperature.

The spectral content of the oscillation was measured with a spectrometer shown in Figure 5-6. For comparison, room temperature luminescence and absorption of the Fe:ZnSe crystal are also depicted in the Figure 5-6. The absorption and the emission bands of Fe:ZnSe overlap in the 3500-5000 nm spectral range. A small shift of the oscillation spectrum from 4300 nm at 236 K to 4370 nm at room temperature is due to the absorption band broadening with the increase of temperature. Figure 5-7 shows the temporal profiles of the pump and Fe:ZnSe laser oscillation pulses measured by HgCdTe detector (PC-10.6, Boston Electronics) with response time shorter than 1 *ns*. Fe:ZnSe oscillation pulses have 15 *ns* duration at FWHM for 20 *ns* pump pulse duration. It is important to note that due to a strong gain in Fe:ZnSe the oscillation and pump pulses nicely overlap. The observed 10 *ns* Fe:ZnSe oscillation delay with respect to the beginning of the pump pulse is comparable with the total pulse duration. Therefore, the increase of the pump pulse duration could be one of the pathways for improved efficiency and output energy of Fe:ZnSe lasers. It can be realized by increasing of the cavity length of the pump Er:Cr:YSGG laser. Spatial distribution of the Fe:ZnSe laser oscillation was measured by using knife-edge method. The output radiation of Fe:ZnSe laser featured Gaussian profile with a diameter d=0.172 mm at $1/e^2$ level. M-squared has been measured as shown in Figure 5-7. Spatial distribution of Fe:ZnSe laser oscillation in terms of distances from the crystal which shows well distributed Gaussian distribution estimates M^2=2.6.

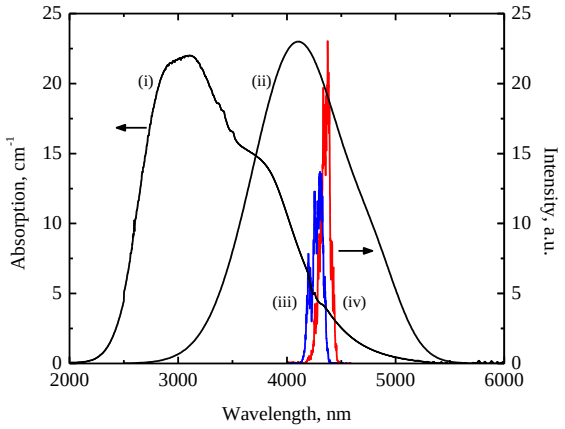

Figure 5-6. RT absorption (i); RT luminescence spectra (ii) as a reference; Fe:ZnSe laser spectra at 236 K (iii) and 300 K (iv).

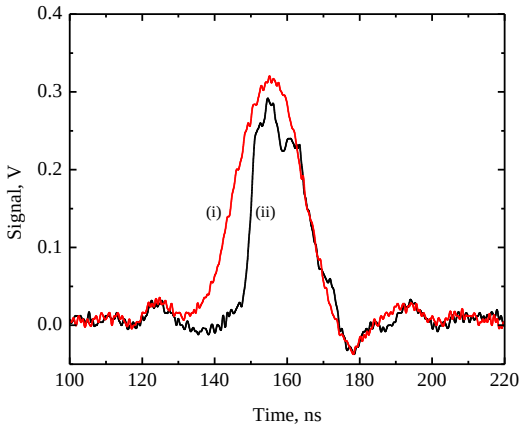

Figure 5-7. Temporal profiles of the pump (i) and gain-switched Fe:ZnSe laser (ii) pulses.

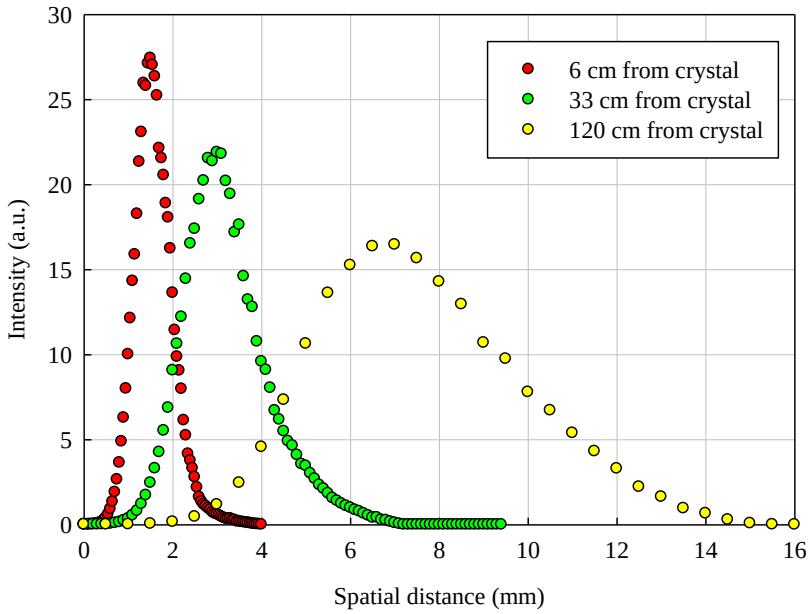

Figure 5-8. Spatial distribution of Fe:ZnSe laser oscillation.

5.2 Lasing via effective Co→Fe energy transfer in ZnS

High gain in the highly doped Co:Fe:ZnS crystals allowed us to test the lasing properties of this crystal under 1.56 μm pumping even without an external cavity. For this experiment we used Co:Fe:ZnS crystals (10x10x1.2 mm^3) with $6x10^{18}$ cm^{-3} and $10x10^{18}$ cm^{-3} concentrations of cobalt and iron, respectively. Crystal surfaces (10x10 mm) were polished in the Laser Lab using Aluminum Oxide polyester film. The key element of the pump laser was an injection seeded, single frequency Q-switched Nd:YAG laser (GCR-230-10, Spectra Physics) with a maximum output energy of 1.5 J at 1.064 μm, a linewidth of 0.003 cm^{-1}, 10 ns pulse duration and a repetition rate of 10 Hz. The 1.064 μm Nd:YAG radiation after passing through an optical isolator was focused by a 25 cm lens into a 50 cm long Raman cell filled with D_2 at a pressure of 600 psi. In backscattering geometry the output energy of the first Stokes line at 1.56 μm exceeded 300 mJ with 7 ns pulse duration at FWHM.

Pump radiation was slightly focused in the spot with *d*~3mm diameter. The crystal was placed in the Close-Cycle Refrigerator operating in 14K-300K temperature range.

Figure 5-9 shows luminescence spectra of several crystals measured at 14K. First plot demonstrates typical Co^{2+} luminescence under 1.56 μm excitation with a characteristic luminescence peaks at around 2800 and 3100 nm. The third plot shows luminescence spectra of the Co:Fe:ZnS crystal with a low iron concentration $0.5x10^{18}$ cm^{-3} under the same 1.56 μm excitation. As one can see from this graph, in addition to Co^{2+} luminescence, there is a strong Fe^{2+} luminescence with characteristic peaks at 3440 nm, 3570nm, and 3820nm. For comparison, the luminescence of the Fe:ZnS sample

under direct excitation of the iron ions at 2.9 μm measured at 14K is depicted in the second graph. The fourth graph shows luminescence spectra of the Co:Fe:ZnS crystal with iron concentration 50 times bigger under 1.56 μm excitation. As one can see, there is no Co^{2+} luminescence in this crystal. The measured luminescence spectrum shows only Fe^{2+} bands slightly red-shifted in comparison with the spectrum of the low doped sample. This result proves that there is a fast energy transfer from Co^{2+} to Fe^{2+} ions in this crystal and we used this crystal for the following laser experiments.

Two basic experiments on pump energy dependence of luminescence kinetics and luminescence spectra were performed to demonstrate Fe^{2+} lasing via effective energy transfer from the Co^{2+} ion. Positive feedback for Fe oscillation was realized due to Fresnel reflections from the crystal facets provide 18% feedback reflectivity from each surface. The large resonator Fresnel Number $N_F = d^2/L\lambda \sim 10^4$ provides minimum diffraction losses in the cavity.

The results of the experiments are shown in the Figure 5-10. Figure 5-10A demonstrates PL spectra of Co:Fe:ZnSe crystal for different pump energies. As one can see in the Figure, at low pump energy the measured PL spectra were typical for the iron luminescence. The dependence of PL spectrum profile on pump energy demonstrated a threshold behavior accompanied by the appearance of a stimulated emission band around 3850 nm as shown in Fig. 5-10.

The change of the luminescence profile above laser threshold accompanied by shortening kinetics of the luminescence is shown in the Figure 5-10B. For low energy pumping, one can see low temperature Fe^{2+} kinetic with luminescence rise time $\tau \sim 1$ μs followed by exponential decay with a lifetime $\tau \sim 2.5$ μs. Above laser threshold, the

kinetics demonstrate typical laser spike with ~200 *ns* pulse duration followed by luminescence kinetics. The threshold dependence of the emission, significant line narrowing, and lifetime shortening are clear evidence of Co:Fe:ZnSe lasing via Co→Fe energy transfer mechanism.

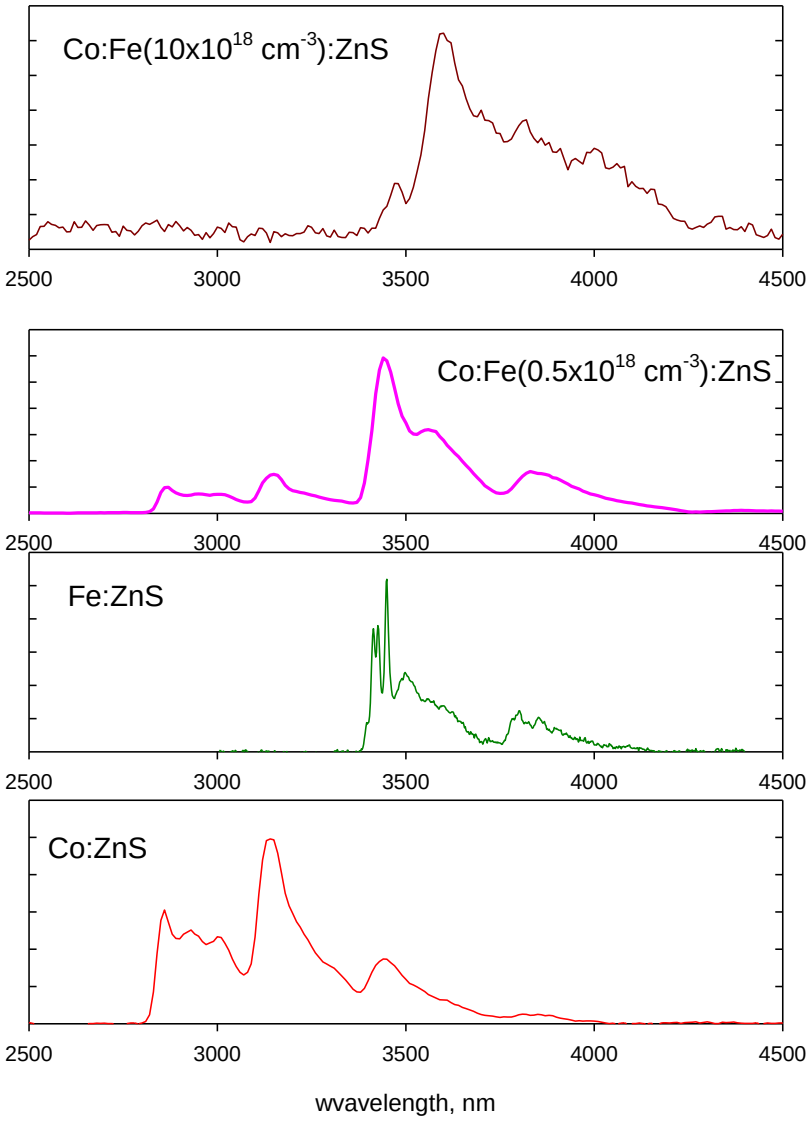

Figure 5-9. Mid-IR luminescence spectra of the iron and cobalt doped crystals at T=14K.

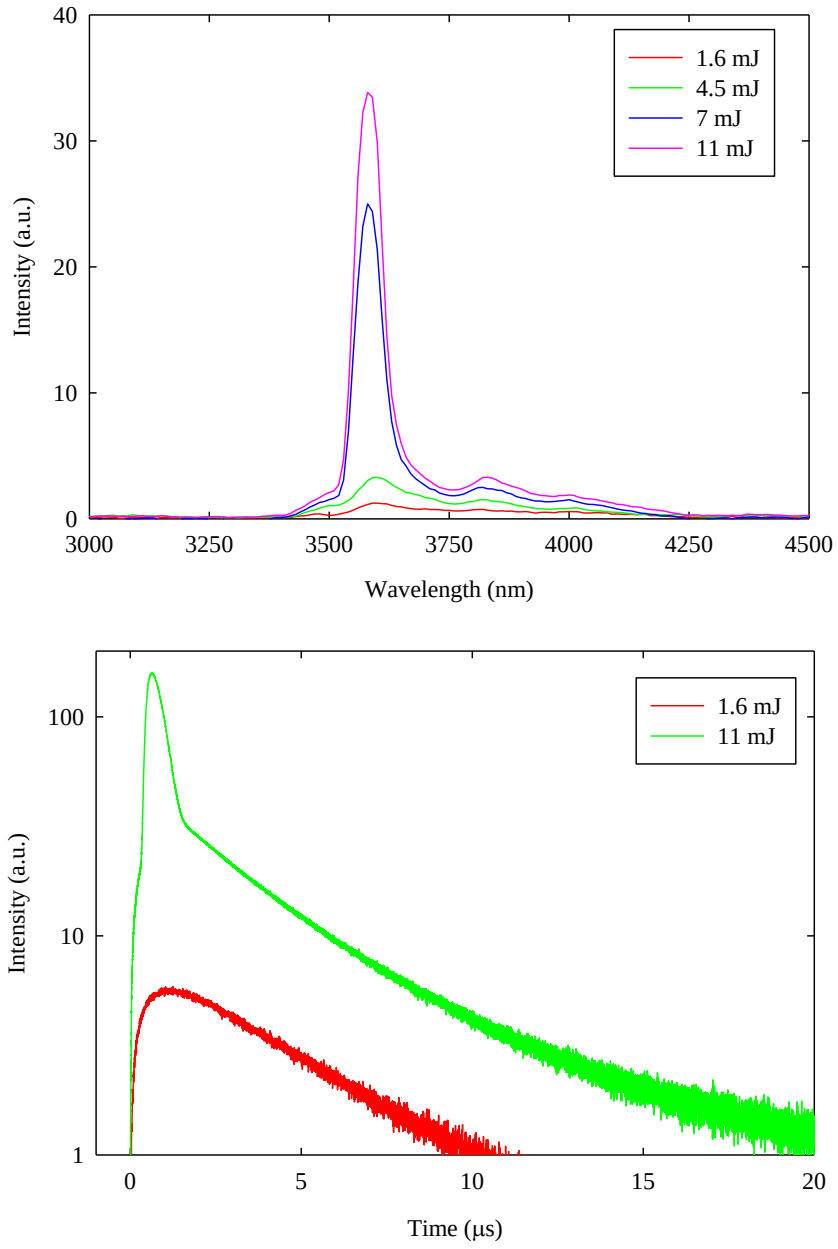

Figure 5-10. A) Mid-IR luminescence spectra of the Co:Fe:ZnS crystal at different pump energies at T=14K, B) Co:Fe:ZnS crystal PL kinetics for different pump energies below (red) and above (pink) laser threshold.

5.3 Summary

1. Summarizing, we have demonstrated that post-growth thermal-diffusion from the metal phase enables fabrication of highly doped, high optical quality Fe:ZnSe gain elements for mid-IR laser applications.
2. We report a four-fold increase of output energy of the gain-switched Fe:ZnSe lase r over the prior art. Under Q-switched Er:Cr:YSGG (2.8 μm) laser excitation (pump energy 33 mJ, energy density 0.35 J/cm^2, pulse duration 20 *ns*, repetition rate 6.7 Hz) the maximum output energy reached 4.7 mJ @ 4.3 μm and 3.6 mJ @ 4.37 μm at 236 K and 300 K, respectively, and was limited only by available pump energy.
3. Threshold was about 8 mJ and was practically unchanged over studied temperature range. The laser slope efficiencies decreased from 19 % to 16 % with an increase of temperature from 236 to 300 K. The maximum peak power obtained was 0.3 MW at 4.3 μm.
4. The new excitation mechanism for Fe^{2+} lasers via the energy transfer from Co^{2+} to Fe^{2+} was demonstrated in the cavity with a positive feedback from the crystal fac ets. It opens new pathway for pumping mid-IR Fe based lasers with the use of commercially available near-IR pump lasers.

CHAPTER 6

CONCLUSIONS

6.1 Conclusions

The current types of Mid-IR lasers such as optical parameter oscillator (OPO) and quantum cascade laser (QCL) suffer from drawbacks like limited power and difficulty to operate at room temperature. Whereas, lasers based on group II–VI compounds doped by transition metals (for example Fe doped binary and ternary chalcogenides), can provide very high power levels at good beam quality and high optical density, but achieving these in reality was a challenge. Each of the experiments in the last two chapters is about the progress in a new direction of study that could be followed to develop our understanding of how to fabricate the transitional metals (TM's) on or in II-VI semiconductors and to characterize their optical properties. First, we presented our work on controlling the concentration of impurities in ZnSe and ZnS using post-growth thermal diffusion. It was realized that pre-cleaning method played crucial roles in diffusion process. Second, we explored how the luminescence lifetime could be tailored by changing the iron concentrations in ZnSe and ZnS with temperature variations. Thirdly, we have found optimal iron concentration in ZnSe as an active gain-medium. Also, it was found that cobalt excited Fe:ZnS may be utilized as a gain medium at low temperature. Finally, we

have designed the 4.3μm Fe:ZnSe laser at room temperature by adopting an efficient fabrication technique based on post-growth thermal diffusion.

The following lists are main achievements during the academic years at Center for Optical Sensors and Spectroscopies (COSS) and Department of Physics, University of Alabama at Birmingham.

1. The fabrication of high optical dense Fe in ZnSe from metal phase and optimization of fundamental diffusion parameters have been suggested by post-growth thermal diffusion of active impurities (Fe) in II-VI crystals grown by evaporation method. The luminescence kinetics measured at different temperatures for Fe^{2+} ions concentration varied from $5.82x10^{18}$ to $85x10^{18}$ ions/cm^3 showed that Fe concentration quenching in ZnSe crystals occurred between 38-$85x10^{18}$ /cm^3 ranges where the lifetime has dropped by about 2 times. This result was presented as " Optically dense Fe:ZnSe crystals for energy scaled gain switched lasing" at *Photonics West 2010* [15].
2. Post-growth thermal-diffusion from the metal phase enables fabrication of highly doped, high optical quality Fe:ZnSe gain elements for mid-IR laser applications. We reported a fourfold increase of output energy of the gain-switched Fe:ZnSe laser over the prior reported results. Under Q-switched Er:Cr:YSGG (2.8 μm) lase r excitation (pump energy 33 mJ, energy density 0.35 J/cm^2, pulse duration 20 ns, rep. rate 6.7 Hz) the maximum output energy reached 4.7 mJ @ 4.3 μm and 3.6 m J @ 4.37 μm at 236 K and 300 K, respectively, and was limited only by available pump energy. Threshold was about 8mJ and was practically unchanged over studi ed temperature range. The laser slope efficiencies decreased from 19 % to 16 % w

ith an increase of temperature from 236 to 300 K. The maximum peak power obtained was 0.3 MW at 4.3 μm. this result was presented at *Photonics West 2011* and at *The Conference on Lasers and Electro-Optics (CLEO) 2011*, and published in *Optics Letters* [17,93,89].

3. The concentration quenching in the Fe:ZnSe crystal is not significant in comparison with a phonon quenching at room temperature up to ~10^{20} cm^{-3} iron concentration. We also demonstrated an effective $Co^{2+} \rightarrow Fe^{2+}$ energy transfer process which could result in utilization of the more convenient laser pump sources for the iron doped ZnSe lasers. The detailed analysis of spectroscopic characterization of Fe:Co:ZnSe crystals as well as a comparison of the optical and magnetic properties of the highly doped Fe:ZnSe sample will be presented at *16th International Conference on Luminescence* (ICL'11) [94].
4. We introduced the alternative methods for cost-effective fabrication of high quality Fe doped gain materials in II-VI compounds. Iron doping of ZnSe and ZnS polycrystals was performed by thermal diffusion from the iron film made by thermal evaporation process. The Fe concentration quenching rate of Fe:ZnSe was estimated with a slope of 2.4x10^{-20} $\mu s^{-1}cm^3$ at room temperature. We observed that the lifetime-concentration curves differed significantly at 13 and 100 K, and it is determined that the relaxation between optical energy levels of Fe^{2+} can depend on the strong, temperature-dependent concentration quenching in ZnSe. The lifetime and luminescence measurements of Fe:ZnS indicated that the temperature quenching started at 14K for all Fe concentrations. These results have been submitted to '*Journal of luminescence*' [95].

6.2 New Directions

The performance of a Fe:ZnSe laser can be improved by choosing the optimum Fe concentration. As a general guideline, it can be stated that a high doping concentration is desirable for Q-switched operation because this will lead to a high energy storage. For CW operation regime, a lower doping concentration is usually chosen to obtain good beam quality and minimum lasing threshold. In addition, energy transfer due to an unintentional co-dopant may change the characteristics of a desired transition, such as the pumping efficiency and emission lifetime of a particular ion. A more detailed research on absorption, photoluminescence (PL), and time resolved PL measurements due to energy transfer between Co^{2+} and Fe^{2+} ion in diffusion-doped ZnSe is needed to try Co^{2+} co-doping of Fe^{2+}:ZnSe crystals with optimal cobalt and iron concentration since due to Co-Fe energy transfer Co:Fe:ZnSe and Co:Fe:ZnS crystals could be pumped with a convenient alexandrite (740 nm) and/or Er:YAG (1645 nm) excitations. To characterize the efficiency of Co-Fe energy transfer kinetics of luminescence measurements need to be performed as a function of Fe and Co concentration.

LIST OF REFERENCES

[1] “Fabrication and Characterization of Semiconductor Lasers,” in Oproelecfronic Technology and Lighnvave Comnz~inicafions (C. Lin. Ed.), P. J. Anthony, Van Nostrand Reinhold, New York (1989).

[2] “Transverse Mode Control in Semiconductor Lasers,” in Oproelecfronic Technology and LighhVUW Conznznnicarions Sysrenzs (C. Lin. Ed.), K. Kobayashi, Van Nosrrand Reinhold. New York (1989).

[3] “New frontiers in quantum cascade lasers and applications,” F.Capasso et.al, *IEEE J. Select. Topics Quant. Elect*. 6, 931 (2001).

[4] “Far-infrared surface-plasmon quantum-cascade lasers at 21.5 µm and 24 µm wavelengths,” R. Colombelli et.al., Appl.Phys. Lett. 78, 2620 (2001).

[5] “Efficient grating-tuned mid-IR Cr^{2+}:CdSe laser,” McKay, Jason, Kenneth L. Schepler, and Gary Catella, Opt. Lett. 24: 1575-1577 (1999).

[6] “Preparation and Optical Properties of Co-Doped ZnSe Single Crystals,” Yu. F. Vaksman, V. V. Pavlov, Yu. A. Nitsuk, Yu. N. Purtov,A. S. Nasibov, and P. V. Shapkin, Semiconductors, V40, 7 (2006).

[7] “Transition Metal-Doped Zinc Chalcogenides: Spectroscopy and Laser Demonstration of a New Class of Gain Media,” L.D. DeLoach, R.H. Page, G.D. Wilke, S. A. Payne, W. F. Krupke, IEEE J. QE 32 885-895 (1996).

[8] “Solid State Lasers and Applications,” by Alphan Sennaroglu and Umit Demirbas, page 113-162 (2006).

[9] “Absorption and photoluminescence spectroscopy of diffusion doped ZnSe:Cr^{2+},” C.I. Rablau, J.-O. NDAP et al. J. Electronic Materials, Vol. 28, No.6 (1999).

[10] “Pulsed mid-IR Cr^{2+}:ZnS and Cr^{2+}:ZnSe lasers pumped by Raman-shifted *Q* switched neodymium lasers,” K Graham, V V Fedorov, S B Mirov, Maxim E Doroshenko, Tasoltan T Basiev, Yu V Orlovskii, Vyacheslav V Osiko, Valerii V Badikov, and V L Panyutin, Quantum Electronics, Vol 4,1 (2004).

[11] “Cr^{2+}:ZnSe Laser Pumped Utilizing Cr Ionization,” A.Gallian, V.V.Fedorov, L. Luke, I.S. Moskalev, S.B.Mirov, V.V. Badikov, *Technical Digest of Optics in the Southeast* , p. 66, Atlanta, USA (2005).

[12] “Efficient grating-tuned mid-infrared Cr^{2+}:CdSe laser,” J. McKay, K. Schepler, and G.C. Catella, Opt. Lett. Vol 24, Issue 22, 1575 (1999).

[13] “Preparation and optical properties of Co-doped ZnSe single crystals,” Yu.F. Vaksman, V.V. Pavlov, Yu.A. Nitsuk, Yu.N. Purtov, A.S. Nasibov, and P.V. Shapkin, Semiconductors, Vol. 40, 7 (2006).

[14] “3.77-5.05μm Tunable Solid-State Lasers Based on Fe^{2+}-Doped ZnSe Crystals Operating at Low and Room Temperatures”, Vladimir V. Fedorov, Sergey B. Mirov, et al., IEEE J. of Quantum Electronics, Vol. 42, No 9 (2006).

[15] “Optically dense Fe:ZnSe crystals for energy scaled gain switched lasing,” NoSoung Myoung, Vladimir V. Fedorov, Sergey B. Mirov, Proc. SPIE, Vol. 7578, 75781H; doi:10.1117/12.842428 (2010).

[16] “Energy scaling of 4.3μm room temperature Fe:ZnSe laser,” NoSoung Myoung, Dmitri V. Martyshkin,Vladimir V. Fedorov, Sergey B. Mirov, Optics Letters, Vol. 36, Issue 1, pp. 94-96 (2011).

[17] “Energy scaling of room temperature Fe^{2+}:ZnSe gain-switched 4.3μm laser,” NoSoung Myoung, Dmitri Martyshkin, Vladimir Fedorov, Alan Martinez, Sergey B. Mirov, Proc. SPIE, Vol. 7912, 79121C, DOI: 10.1117/12.874980 (2011).

[18] “3.77-5.05μm Tunable Solid-State Lasers Based on Fe^{2+}-Doped ZnSe Crystals Operating at Low and Room Temperatures,” Vladimir V. Fedorov, Sergey B. Mirov, et al., IEEE J. of Quantum Electronics, Vol. 42, No 9 (2006).

[19] “Laser parameters of a Fe:ZnSe crystal in the 85-255K temperature range,” A.A. Voronov, V.I. Kozlovskii, Yu.V. Korostelin, A.I. Landman, Yu.P. Podmar’kov, M.P. Frolov, Quantum Electronics 35(9) 809-812 (2005).

[20] “Room-temperature tunable mid-infrared lasers on transition-metal doped II–VI compound crystals grown from vapor phase,” V.I. Kozlovsky, V.A. Akimov, M.P. Frolov, Yu.V. Korostelin, A.I. Landman, V.P. Martovitsky, V.V. Mislavskii, Yu. P. Podmar’kov, Ya.K. Skasyrsky, and A.A. Voronov, Phys. Status Solidi B, 1-4 (2010).

[21] “4.0-4.5 μm lasing of Fe:ZnSe below 180K, a new mid-infrared laser material,” J.J. Adams, C. Bibeau, R.H. Page, D.M. Krol, L.H. Furu, S.A. Payne, Opt. Lett. 24, 1720 (1999).

[22] “A continuous-wave Fe^{2+}: ZnSe laser,” A.A. Voronov, V.I. Kozlovsky, Yu.V. Korostelin, A.I. Landman, Yu.P. Podmar'kov, Ya.K. Skasyrsky, M.P. Frolov, IEEE J. Quantum Electronics, 38 (12), 1113-1116 (2008).

[23] "3.9-4.8 μm gain-switched lasing of Fe:ZnSe at room temperature," J. Kernal, V.V. Fedorov, A. Gallian, S.B. Mirov, V.V. Badikov, Optics Express, 13, 10608 (2005).

[24] "Efficient lasing in a Fe^{2+}: ZnSe crystal at room temperature," V.A. Akimov, A.A. Voronov, V.I. Kozlovsky, Yu.V. Korostelin, A.I. Landman, Yu.P. Podmar'kov, M.P. Frolov, IEEE J. Quantum Electronics, 36(4), 299-301 (2006).

[25] "Tunable mid-infrared laser properties of Cr^{2+}:ZnMgSe and Fe^{2+}:ZnSe crystals," M.E. Doroshenko, H. Jel´ınkov´a, P. Koranda, J. Sulc, T.T. Basiev, V.V. Osiko, V.K. Komar, A.S. Gerasimenko,V.M. Puzikov, V.V. Badikov, and D.V. Badikov, Laser Phys. Lett., 7, No 1, 38-45 (2010).

[26] "Room-temperature lasing, gain-switched bulk, tunable Fe:ZnSe laser," Helena Jelínková, Petr Koranda, Maxim E. Doroshenko, Jan Šulc, Michal Jelínek, and Miroslav Cech, Tasoltan T. Basiev, Valerii V. Badikov and Dmitri V. Badikov, Proc. SPIE, 7721, 772111; doi:10.1117/12.854304 (2010).

[27] "Supplementtary Investigations of Infrared Spectra," W.W. Coblentz, Carnegie Instit. Wash. Publ. 97, Part VI, p. 57 (1908)

[28] "Paramagnetic resonance and optical spectra of divalent iron in cubic fields. I. Therory," W. Low and M. Weger, Phys. Rev. 118, 1119; 118, 1130 (1960)

[29] "Pulsed Fe^{2+}:ZnS laser continuously tunable in the wavelength range of 3.49-4.65 μm," V.I. Kozlovsky, Yu.V. Korostelin, A.I. Landman, V.V. Mislavskii, Yu.P. Podmar'kov, Ya.K. Skasyrsky, and M.P. Frolov, Quantum Electronics 41, 1, pp.1-3 (2011)

[30] "Isolated iron and chromium recombination centers in ZnS", A. Zakrzewski and M. Godlewski, J.Appl. Phys. 67 (5), 2457-2461 (1990).

[31] "ZnSe:Co^{2+}-nonlinear optical absorber for giant-pulse eye-safe lasers," Z.Mierczyk, A. Majchrowski, I.V. Kityk, and W. Gruhn, Optics & Laser Tech. V. 35, Issue 3, p. 169-172 (2002).

[32] "Auger-type excitation and de-excitation processes in rare-earth and transition metal doped semiconductors," J. of Alloys and compounds, 300-301, 23-31 (2000).

[33] "The chromium impurity photogeneration transitions in ZnS, ZnSe and ZnTe," J. Phys. C, Solid St. Phys., v 13, N 35, 6537-6645 (1980).

[34] "Transition Metal Doped Zinc Chalcogenides: Spectroscopy and Laser Demonstration of a New Class of Gain Media," L. D. DeLoach, R.H. Page, G.D. Wilke, S. A. Payne, and W. F. Krupke, *IEEE J. Quantum Electron* 32 885-895 (1996).

[35] "Cr^{2+}-Doped Zinc Chalcogenides as Efficient, Widely Tunable Mid-Infrared Lasers,"

R. H. Page, K. I. Schaffers, L. D. DeLoach, G. D. Wilke, F. D. Patel, J. B. Tassano, S. A. Payne, W. F. Krupke, K. T. Chen, A. Burger, *IEEE J. Quantum Electron* 33, 4, 609-617 (1997).

[36] "Continuous-wave broadly tunable Cr^{2+}: ZnSe laser," G. J. Wagner, T. J. Carrig, R. H. Page, K. I. Schaffers, J. O. Ndap, X. Ma, A. Burger, Opt. Lett. **24**, 19-21 (1999).

[37] "Efficient laser operation and continuous-wave diode pumping of Cr^{2+}:ZnSe single crystals," A.V. Podlipensky, V.G. Shcherbitsky, N.V. Kuleshov, V.I. Levchenko, V.N. Yakimovich, M. Mond, E. Heumann, G. Huber, H. Kretschmann and S. Kuck, Appl. Phys. B72, 253 (2001).

[38] "Infrared luminescence and application of a vibronic-coupling Hamiltonian to the level structure of CdTe:Fe^{2+}," Phys. Rew. B, vol. 50, No.8 (1994).

[39] "Efficient pulsed Cr^{2+}:CdSe laser continuously tunable in the spectral range from 2.26 to 3.61 μm," V.A. Akimov, V.I. Kozlovskii, et al., Quantum Electronics, 38(3), 205-208 (2008).

[40] J.H. Haanstra, in Proc. of International Conference on II-VI semiconductor Compounds, edited by D.G.Thomas, pp.207, New York (1967).

[41] "Luminescence and related optical properties of iron ions in II-VI compounds," G. Roussos, H.-J. Schulz, and M. Thiede, J. Lumin. v31-32, 409-411 (1984).

[42] "Trends in Optics and Photonics," A.J.S. McGonigle, D.W.Coutts, C.E. Webb, ed. By M. J. Fejer, H. Injeyan, U. Keller, OSA Vol. 26, pp.115-117 (OSA, Washington, DC 1999).

[43] "Wavelength-Dependent Collagen Fragmentation during Mid-IR Laser Ablation," Yaowu Xiao**,** Mingsheng Guo**,** Kevin Parker and M. Shane Hutson, Biophysical Journal, Volume 91, Issue 4, 1424-1432 (2006).

[44] "Acousto-optic mode-locking of a Cr^{2+}:ZnSe laser," T. J. Carrig, G. J. Wagner, A. Sennaroglu, J. Y. Jeong, and C. R. Pollock, in Advanced Solid State Lasers, H. Injeyan, U. Keller, and C. Marshall, eds., vol. 34, pp. 182–187 (OSA, Washington DC, 2000).

[45] "Efficient laser operation and continuous-wave diode pumping of Cr^{2+}:ZnSesingle crystals," A. V. Podlipensky, V. G. Shcherbitsky, N. V. Kuleshov, V. I. Levchenko, V. N.Yakimovich, M. Mond, E. Heumann, G. Huber, H. Kretschmann, and S. Kuck, Appl. Phys. B 72(2), 253–255 (2001).

[46] "Laser oscillation at 3.53 μm from Fe^{2+} in n-InP:Fe," P. B. Klein, J. E. Furneaux, and R. L. Henry, Appl. Phys. Lett. 42, 638 (1983).

[47] “Efficient IR Fe:ZnSe laser continuously tunable in the spectral range from 3.77 to 4.40μm,” V. A. Akimov, A. A. Voronov, V. I. Kozlovskii, Yu. V. Korostelin, A. I. Landman, Yu. P. Podmar'kov,M. P. Frolov, Quantum Electron. 34(10), 912-914 (2004).

[48] “Cr^{2+}:ZnSe laser pumped by 1.66μm or 1.97μm radiations,” H. Jelinkova, P. Koranda, et al., Laser physics letters, Vol. 4, issue 1, p23-29 (2006).

[49] “Iron and chromium impurities in ZnSe as centers of nonradiative recombination,” M. Surma and M. Godlewski, Phys. Rev. B, Vol. 50, No. 12 (1994).

[50] “Heat treatments of ZnSe starting materials for physical vapor transport,” Ching-Hua Su, W. Palosz, et al., J. Crystal Growth, Vol. 192, p386-394 (1998).

[51] “Pulse laser deposition growth and spectroscopic perperties of chrominum doped ZnS crystalline thin films,” S.B. Mirov, S. Wang, V.V. Fedorov, and R.P. Camata, Proc. Advanced Solid State Photonics, Vol. 5332, Optical Society of America, Santa Fe, NM, p. WB15 (2004).

[52] “Heavy Cr doping of ZnSe by molecular beam epitaxy,” B.L Vanmil, A.J. Ptak, L. Bai, L. Wang, M. Chirila, N.C. Giles, T.H. Myers, and L. Wang, J. Electron. Mater. 31, 770-775 (2002).

[53] “Vapor growth and characterization of Cr-doped ZnSe crystals,” C.-H. Su, S. Feth, M.P. Volz, R. Matyi, M.A. George, K. Chattopadhyay, A. Burger, and S.L. Lehoczky, J. Cryst. Growth 207, 35-42 (1999).

[54] “Cr^{2+}-doped zinc chalcogenides as efficient, widely tunable mid-infrared lasers,” R.H. Page, K.I. Schaffers, L.D. DeLoach, G.D. Wilke, F.D. Patel, J.B. Tassano, S.A. Payne, W.F. Krupke, K.-T. Chen, and A. Burger, IEEE J. Quantum Electronics, Vol. 33. No. 4, 609 (1997).

[55] “Vapour growth of II-VI single crystals doped by transition metals for mid-infrared lasers,” V.A. Akimo, M.P. Frolov, Y.V. Korostelin, V.I. Kozlocsky, A.I. Landman, Y.P. Podmar’jic, and A.A. Voronov, Phys. Stat. So. (c) 3, No. 4, 1213-1216 (2006).

[56] “High-brightness blue and green light-emitting diodes,” D.B Eason, Z. Yu, W.C. Hughes, W.H. Roland, C. Boney, JW. Cook, J.F.Schetzina, G. Cantwell and W.C. Harsch,, Appl. Phys. Lett. v66, 115 (1995).

[57] “Computer analysis and optimization of physical and material parameters of the blue laser diode,” D.S Patil and D. K. Gautam, Optics Commun., v201, pp. 413-423 (2002).

[58] “Optical characterization of native defects in ZnSe substrate,” K. Youshino, H. Mikami, et.al, Physica B, V 302-303, pp. 299-306 (2001).

[59] “Doping in ZnSe, ZnTe, MgSe, and MgTe wide-band-gap semiconductor.” D.J. Chadi, Phy. Rev. Lett.V 72, Issue 4, pp. 534-537 (1994).

[60] “Infrared luminescence and vibronic coupling in ZnTe:Fe^{2+},” H. -J. Schulz, M. Thiede, U.W. Pohl, J. Rivera-Iratchet and M.A. de Orue, etal., Z. Phys. B v 98, pp. 215-221(1995)

[61] “Infrared (2-12μm) solid-sate laser sources: a review,” A.Godard, C.R. Physique 8, 1100-1128 (2007).

[62] “Laser-related spectroscopy of ion-doped crystals for tunable solid state lasers,” S. Kuk, Appl. Phys. B: Lasers and Optics, v72, pp. 515-562 (2001).

[63] “Many-electron multiplet effects in the spectra of 3*d* impurities in heteropolar semiconductors,” by A. Fazzio, M. J. Caldas, and Alex Zunger, Phys. Rew. B V30, No 6 (1984).

[64] “Iron and chromium impurities in ZnSe as centers of nonradiative combination,” M. Surma, M. Godlewski, and T.P. Surkova, Phys. Rev. B 50, 8319-8324 (1994).

[65] “Transition-metal impurities in II–VI semiconductors: characterization and switching of charge states,” J. Kreissl, H.-J. Schulz, J. Crystal Growth, V 161, Issues1-4, pp. 239-249 (1996).

[66] “3.9-4.8 μm gain-switched lasing of Fe:ZnSe at room temperature,” J. Kernal, V.V. Fedorov, A. Gallian, S. B. Mirov, Optics Exp. Vol. 13, No. 26 (2005).

[67] “Absorption saturation analysis of Cr^{2+}:ZnSe and Fe^{2+}:ZnSe,” Huseyin Cankaya, Umit Demirbas, A.K Erdamar and A. Sennaroglu, JOSA B. Vol. 25. Issue 5, pp. 794-800 (2008).

[68] “Fe-based semimagnetic semiconductors with two anions,” A. Mycielski, M. Arciszewska, W. Dobrowolski, A. Łusakowski, K. Dybko, R. Szymczak, and A. Szadkowski, Phy. Rew. B. V. 53, No 16 (1996).

[69] “Two-mode Jahn-Teller effect in the absorption spectra of Fe^{2+} in II-VI and III-V semiconductors, ” O. Mualin, E. E. Vogel, M. A. de Oru´e, L. Martinelli, G. Bevilacqua, and H.-J. Schulz, Phy. Rew. B. V 65, 035211 (2001).

[70] “Diffusion coefficient of Fe^{2+} in single-crystal ZnSe,” N. N. Il’ichev, P.V. Shapkin, E.S. Gulyamova, L.A. Kulesky and A.S. Nasibov, Inorganic Materials, V 46, 2, 112-115 (2010)

[71] “Measurement of Gaussian laser beam radius using the knife-edge technique: improvement on data analysis,” Applied Optics, V. 48, Issue 2, pp. 393-396 (2009).

[72] “Synthesis and characterization of diffusion-doped Cr^{2+}:ZnSe and Fe^{2+}:ZnSe,” U. Demirbas, A. Sennaroglu, M. Somer, Optical Materials **28**, 231-240 (2006).

[73] “Parametric resonance and optical spectra of divalent iron in cubic fields (I. theory),” W. Low and M. Weger, Phys. Rev., vol. 123, pp.1188–1203 (1961).

[74] “Optical absorption of tetrahedral Fe^{2+} ($3d^6$) in Cubic ZnS, CdTe, and $MgAl_2O_4$,” G. A. Slack, F. S. Ham, and R. M. Chrenko, Phys. Rev. B 152(1), 376–402 (1966).

[75] “Thermal diffusion of Cr^{2+} in bulk ZnSe,” J.-O. Ndap, K. Chattopadhyay, O.O. Adetunji, D.E. Zelmon, A. Burger, J. crystal growth,V240, Issues 1-2, pp. 176–184 (2002).

[76] “Infrared Luminescence of Fe^{2+} in ZnS,” Glen A. Slack, B. M. O'Meara, Phys. Rev. 163, 335–341 (1967).

[77] “Crystal-Field Engineering of Solid-State Laser Materials,” B. Henderson, R.H. Bartran, Cambridge University Press, Cambridge, 2000

[78] “Induced-emission cross-sections in neodymium laser glasses,” W. F. Krupke, IEEE J. Quantum Electron. 10, 450 (1974)

[79] “Near infrared luminescence of Ni and Fe doped ZnSe Crystals,” A. Karipidou, H. Nelkowski and G. Roussos, J. Crystal Growth, V. 59, Issue 1-2, pp. 307-311 (1932).

[80] “Crystal field engineering of solid state laser materials,” Brian Henderson and Ralph H. Bartram, Cambridge University Press, pp 196-200 (2000).

[81] “A Theory of Sensitized Luminescence in Solids,” J. Chem, Phys, 21, 836 (1953).

[82] “Energy transfer between Co^{2+} and Fe^{2+} ion sin diffusion-doped ZnSe,” Ming Luo, N.C. Giles, Utpal N. Roy, Yunlong Cui, and Arnold Burger, J. Appl. Phys 98, 083507 (2005).

[83] “Co^{2+}:ZnS and Co^{2+}:ZnSe saturable absorber Q switches,” Tzong-Yow Tsai and Milton Birnbaum, J. Applied Phys., V87, N1 (2000).

[84] “Efficient grating-tuned mid-infrared Cr^{2+}:CdSe laser,” J. McKay, K. Schepler, and G.C. Catella, Opt. Lett. Vol 24, Issue 22, 1575 (1999).

[85] “Preparation and optical properties of Co-doped ZnSe single crystals,” Yu.F. Vaksman, V.V. Pavlov, Yu.A. Nitsuk, Yu.N. Purtov, A.S. Nasibov, and P.V. Shapkin, Semiconductors, Vol. 40, 7 (2006).

[86] “Laser parameters of a Fe:ZnSe laser crystal in the 85-255K temperature range,” A. A. Voronov, V. I. Kozlovskii, Yu. V. Korostelin, A. I. Landman, Yu. P. Podmar'kov, M. P. Frolov, Quantum Electron. 35(9), 809-812 (2005).

[87] “Room-temperature tunable mid-infrared lasers on transition-metal doped II–VI compound crystals grown from vapor phase,” V.I. Kozlovsky, V.A. Akimov, M.P. Frolov, Yu.V. Korostelin, A.I. Landman, V.P. Martovitsky, V.V. Mislavskii, Yu. P. Podmar’kov, Ya.K. Skasyrsky, and A.A. Voronov, Phys. Status Solidi B, 1-4 (2010).

[88] “A continuous-wave Fe^{2+}: ZnSe laser,” A.A. Voronov, V.I. Kozlovsky, Yu.V. Korostelin, A.I. Landman, Yu.P. Podmar'kov, Ya.K. Skasyrsky, M.P. Frolov, IEEE J. Quantum Electronics, 38 (12), 1113-1116 (2008).

[89] “Energy scaling of 4.3μm room temperature Fe:ZnSe laser,” NoSoung Myoung, Dmitri V. Martyshkin, Vladimir V. Fedorov, and Sergey B. Mirov, Optics Letters, Vol. 36, Issue 1, pp. 94-96 (2011).

[90] “Room-temperature lasing, gain-switched bulk, tunable Fe:ZnSe laser,” Helena Jelínková, Petr Koranda, Maxim E. Doroshenko, Jan Šulc, Michal Jelínek, and Miroslav Cech, Tasoltan T. Basiev, Valerii V. Badikov and Dmitri V. Badikov, Proc. SPIE, 7721, 772111; doi:10.1117/12.854304 (2010).

[91] “Electrooptically Q-switched mid-infrared Er:YAG laser for medical applications,” A. Zajac, M. Skorczakowski, J. Swiderski, P. Nyga, Optics Express, Vol. 12, Issue. 21, pp. 5125-5130 (2004).

[92] “Diffraction Loss and Selection of Modes in Maser resonators with Circular Mirrors,” T. Li, Bell System tech. J. 44, 917 (1965).

[93] “High energy gain-switched Mid-IR lasers based on Cr and Fe doped ZnSe”, NoSoung Myoung, Mikhail S. Mirov, Vladimir V. Fedorov, and Sergey B. Mirov, *the Conference on Lasers and Electro-Optics* (CLEO), Baltimore, Maryland, May 1-6 (2011).

[94] “Energy transfer and concentration quenching in Iron and Cobalt co-doped ZnSe Laser Materials,” NoSoung Myoung, Dmitri V. Martyshikin, Vladimir V. Fedorov, and Sergey B. Mirov, *16th International Conference on Luminescence* (ICL’11), Ann Arbor, Michigan, USA, June 26-July 1 (2011).

[95] “Temperature and concentration quenching of Fe^{2+} in ZnSe and ZnS laser crystals,” NoSoung Myoung, Vladimir V. Fedorov, and Sergey B. Mirov, *submitted to* “*Journal of luminescence*” (2011).